（千葉大学審査学位論文）

Molecular Approach of the Interfacial Design for Platinum, Carbon, and Polymer Electrolyte in Polymer Electrolyte Fuel Cells

2014 年 3 月

千葉大学理学研究科

基盤理学専攻　化学コース

岡　和輝

Contents

Abstract

Fuel cells which are expected next generation energy produce device, it is essential for increasing electrical power generation efficiency. For the realization, it is needed to technique forming activity site over catalyst effectively. The activity site in PEFC is in triple phase boundary where catalyst surface, proton conductive polymer, reactant gas are gather together. Triple phase boundary have been obtaining experientially. Then, four approach is attempted in this work.

First approach is decreasing electrical conductive loss to control Pt–C interface. Platinum nanoparticles have been reported with mean size of between 1.5 and 7 nm supported on carbon. The contact between Pt nanoparticles and C has never been controlled and monitored nanoscopically. In this paper, stable Pt nanoparticles with mean size of 1.2 nm were synthesized embedded on/in C matrix catalytically produced from acetylene over the Pt nanoparticles. The replica-Pt-C composite was synthesized inside the ordered mesopores (2.7 nm) of Al-MCM-41 followed by removal of template. The contact between Pt nanoparticle and C was experimentally observed by high energy-resolution Pt L_2-edge XANES spectra tuned to 11065.7 eV, at lower energy by 5 eV than the Pt $L\beta_1$ peak top for the replica-Pt-C pressed to electrolyte polymer (Nafion). The spectra were nicely reproduced in theoretical spectrum using *ab initio* multiple scattering calculations for the interface Pt site between cubo-octahedral Pt_{38} and graphite layers. Other Pt sites detected in state-selective Pt L_2-edge XANES were exclusively metallic for replica-Pt-C/Nafion either in air or in H_2. Thus-characterized replica-Pt-C composite was tentatively tested as cathode of H_2-air polymer electrolyte fuel cell in comparison to commercial 20 wt% Pt/Vulcan XC-72 as cathode. The

improvement of Pt dispersion stabilized on/in C matrix, effective contact of Pt with C, and diffusion of fuel O_2 in a few nanometers of replica-Pt-C powder was suggested.

Second approach is increasing gas diffusion to make carbon architecture sterically-bulky. The replica Pt–C composite was synthesized utilizing silica template having three-dimentional ordered pore. Carbon structure of that is slightly greater graphene planar direction than synthesized from silica template having one-dimentional ordered pore, and pore volume of that is 1.3 times larger than. As probe test for diffusing reactant gas, N_2 generation in N_2O decomposition reaction is 1.5 times higher than replica Pt–C composite synthesized from silica template having one-dimentional ordered pore. However, it is necessary to examine replica Pt–C composites utilizing cathode in PEFC, particularly.

Third approach is evaluation for forming triple phase boundary to track electronic state for surface of platinum particle. Based on synchrotron X-ray absorption fine structure to monitor directly the status of catalysts in PEFCs, it was found that Pt sites were reduced to Pt^0 by alcohols contained in polymer electrolyte dispersion solution during the preparation of cathode of PEFC. As in membrane electrolyte assembly, only the Pt sites not covered by polymer electrolyte reoxidized to $Pt^{2+/4+}$. Thus, the interface between Pt and polymer electrolyte was evaluated.

Fourth approach is to functionalize carbon surface with sulfonate/sulfate group to conduct protons. Similar level of proton conductivity was observed in current-voltage dependence compared to using polymer electrolyte, but polymer electrolyte was advantageous to lose less voltage for activation. Based on this comparison, optimum catalyst on cathode is proposed comprising surface sulfonate/sulfate group on carbon mixed with polymer electrolyte. Further optimization of cathode catalyst is proposed

to functionalize carbon with sulfonate group linked to fluorocarbon branch.

Chapter 1

Introduction

1.1 Fuel cells

1.1.1 Positioning the fuel cells in electrical power generation method

In recent years, global warming and energy issues would be typical topic in environmental issues. Main reason of global warming is assumed increasing CO_2 which is greenhouse effect gas[1]. The 67% of the world's electrical energy in 2009 was produced by combustion of fossil fuels with releasing CO_2[2]. Without releasing CO_2, nuclear electricity generation was 14% of the world's electrical energy[2]. The global shift of energy production from fossil fuels to renewable energy sources requires higher efficiency and reliability.

In fuel cells (FCs), erectric energy was produced with reacting H_2 and O_2. This is sustainable energy system for the next generation because environmentally hazardous substances were not emitted such as CO_2, NOx, and SOx rasing global warming or acid rain. Moreover, fuel H_2 can be produced by not only also petroleum but also water or plants. Hence, FCs is core technology making sustainable society after energy paradigm shift. In Japan, ENE・FARM is being sold for home use[3-5] and fuel cell vehicle (FCV) equipped with PEFC is determined to release in 2015[6-8].

As with a general battery cell, FCs directly converts chemical energy into electrical energy, but distinguish other battery cells. Whereas the battery cells performing in batch system is not suitable for growing in size, FCs performing in flow system can grow in size easily. Then, FCs is not so much battery cell as electricity generator

taxonomically.

FCs is harnessed electron transfer as energy, with fuel burning reaction separating to fuel oxidation in anode and O_2 redoction in cathode using electrolyte. FCs are various types. Typical FCs are explained in next section.

1.1.2 Types of FCs

1.1.2-1 Distinguishing of fuels

Fuels are used H_2 or methanol. There are emitted quite low CO_2 compared with fossil fuels. Using H_2 as fuel, theoretical cell voltage is 1.23 V and theoretical energy conversion is high (83%)[9]. However, gas phase fuel is difficult strage because of the volume. There are various researches such as hydrogen storing alloy[10,11] and hydrogen chemi-/ad-sorptionmaterial[12-15].

Using methanol as fuel, FCs is called direct methanol fuel cell (DMFC) and theoretical cell voltage is 1.21 V. This is slightly lower than using H_2. In running DMFC, it needs to stack serially hundreds of cells for obtaining requires cell voltage. Even 2% low voltage makes constraction cost enormous. There is another probrem in electrolyte. Metahol is through out electrolyte materials and makes output decreasing. Nevertheless, applying DMFC to mobile phone is being studied because liquid fuel has high mobility[16].

1.1.2-2 Distinguishing of electrolyte

Table 1-1 shows feature of each FCs due to the difference of the electrolyte and Figure 1-1 illustrate composition of the each FC type.

1.1.2-2a　Polymer electrolyte fuel cell (PEFC)

PEFS is utilizing polymer type electrolyte.　DMFC also fall into this category. Operating temperature is 273－373 K becase polymer electrolyte need liquid water to deliver proton.　In order to operate low temperature and be small, PEFC have been studing application for home electric generator and fuel cell vehicle (FCV)[17]. Exhaust heat offen use for hot-water supply and room heating.　Total energy efficiency in best conditions is 70－80%.

Table 1-1.　FCs types[9]

	Polymer electrolyte fuel cell (PEFC)	Phosphoric acid fuel cell (PAFC)	Molten carbonate fuel cell (MCFC)	Solid oxide fuel cell (SOFC)
Electrolyte	Polymer electrolyte (Solid)	Phosphoric acid solution (Liquid)	Molten carbonate (Liquid)	Ceramic electrolyte (Solid)
Operative temperature	r.t－373 K	423－473 K	923－973 K	973－1273 K
Fuel	H_2 Methanol Reformed natural gas Reformed gasoline	Reformed natural gas Reformed LPG Reformed methanol	Natural gas LPG Coal gas	Natural gas LPG Coal gas
Generating efficiency	30－40% (reformed gas)	35－45%	45－65%	45－65%
Feature	・Low operating temperature ・Mobility ・Easy start-and-stop	・In practical use	・High efficiency ・Internal reforming	・High efficiency ・Internal reforming ・Utilization of exhaust heat

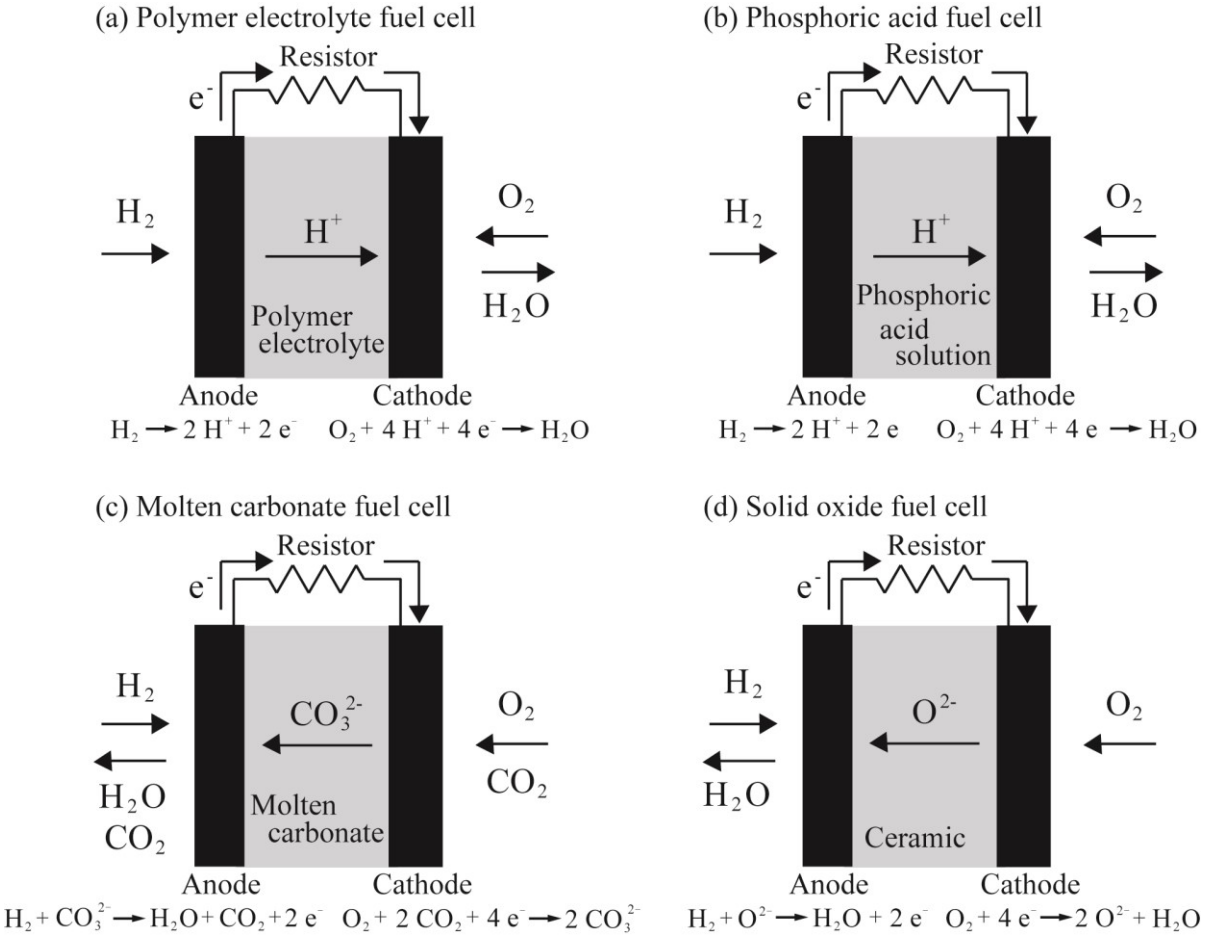

Figure 1-1. Composition of FCs

1.1.2-2b Phosphoric acid fuel cell (PAFC)

PAFC is utilizing porous membrane impregnated phosphoric acid solution as electrolete. This type electrolyte can not perfectly separate between anode side and cathode side. Thus, PAFC is difficult to obtain high performance and to downsize. However, it is practically for large generator for business use in 1992 because of simplicity manufacture[9].

1.1.2-2c Molten carbonate fuel cell (MCFC)

The electrolyte in MCFC is alkali metal carbonate such as molten mixture of

lithium and sodium carbonate. MCFC is high efficient cell to operate high temperature (923－973 K). Although material which has high durability for molten carbonate is expensive. There are hopes that inexpensive material for MCFC is developped.

1.1.2-2d Solid oxide fuel cell (SOFC)

SOFC is utilizing ion-conducting ceramic such as perovskite oxide for electrolyte. SOFC is high efficient cell to operate high temperature (973－1273 K) but requires long heating time from ambient temperature to operating temperature. Then, SOFC is suitable for long term continuous running. There are hopes to develop inexpensive material which has high dulability for high temperature.

1.2 Cathode catalyst in PEFC

The catalyst in PEFC is too expensive because of utilizing platinum. When FCV is begun commercial production, price of FC system in FCV is estimated $ 8,000/80 kW and that of 30% is catalyst price[18]. It is too expensive to stimulate consumer appetite. In PEFC, oxgen reduction reaction (ORR; $O_2 + 4H^+ + 4e^- \rightarrow 2H_2O$) over cathode has high overpotential, and is rate-limiting reaction[19]. Therefore, it needs to increase the ORR activity over cathode catalyst and to go up electrical generating capacity.

1.3 Catalyst layer in PEFC

ORR is need electron, O_2, and proton. In catalyst layer, these are derivered through carbon (solid phase), hollow (gas phase), polymer (pseudo-liquid phase), respectively. Then, active site is triple phase boundary[9]. Meanwhile, these phases block the role of derivering reactants each other phase. For instance, electrons can not

pass through the polymer and hollow. If there is shortage of reactants , cell voltage fall to a low level. Then, reactants derivery path in catalystlayer are need to highly design and control for obtaining high performance output.

1.4 References

[1] Intergovernmental Panel on Climate Change (2001) *Climate Change 2001, Synthesis Report Summary for Policymakers* (Intergovernmental Panel on Climate Change, Washington, DC), Third Assessment Report.

[2] IEA, World Energy Outlook 2011 (OECD, Paris)

[3] Introduction of Household Fuel Cell Cogeneration System, Panasonic Corporation, http://panasonic.co.jp/ap/FC/index.htm, Jan 14, 2014

[4] Introduction of Household Fuel Cell Cogeneration System, JX Nippon Oil & Energy Corporation, http://www.noe.jx-group.co.jp/lande/product/fuelcell/, Jan 14, 2014

[5] Introduction of Household Fuel Cell Cogeneration System, TOSHIBA FUEL CELL POWER SYSTEMS CORPORATION, http://www.toshiba.co.jp/product/fc/, Jan 14, 2014

[6] Roadmap for Fuel Cell Vehicle, Fuel Cell Commercialization Conference of Japan, http://fccj.jp/pdf/22_csj.pdf , Jan 14, 2014

[7] Toyota FCV Concept, TOYOTA MOTOR CORPORATION, http://www.toyota-global.com/tokyoms2013/fcv/, Jan 14, 2014

[8] News releases, “ELEVEN MINUTES, 58 SECONDS AND ZERO EMISSIONS”, NISSAN MOTOR CORPORATION,

http://www.nissan-global.com/EN/NEWS/2008/_STORY/080723-02-e.html., July 23, 2008

[9] Takasu et al., Fuel Cell Characterization Methods, Kagaku-Dojin, 2005

[10] Ivey et al., J. Mater. Sci., 18(2), 321-347(1983)

[11] Young et al., J. Alloys Compounds, 509(5), 2277-2284(2011)

[12] Reddy et al, Int. J. Hydrogen Energy, 32(17), 4272-4278(2007)

[13] Dillon et al., Nature, 386, 6623, 377-379(1997)

[14] Wang et al., Chem. Soc. Rev, 42, 7, 3088-3113(2013)

[15] Furukawa et al, Science, 341, 6149, Article number 1230444 (2013)

[16] Chen et al., J. Power Sources, 123, 1, 37-42(2003)

[17] Schlapbach et al., Nature, 460, 809-811(2009)

[18] FC System Cost estimation, Department of Energy, America (2008)

[19] Nørskov et al., J. Phys. Chem. B, 108, 46, 17886-17892(2004)

Chapter 2

Replica Pt–C

2.1 Introduction

The control of platinum nanoparticle size between 1.5 and 7 nm supported on carbon is essential in the application to fuel cells[1] and detoxification of exhaust gas from automobiles.[2] Pt nanoparticles on C nanofibers (mean Pt size of 1.7-4 nm),[3,4] C nanotubes (mean Pt size of 2-6.7 nm),[4–10] ordered mesoporous C (mean Pt size of 1.5-3 nm),[11–13] C powder (mean Pt size of 1.6-4.8 nm),[14–17] and spherical C (mean Pt size of 2.9 nm)[18] and Pt monolayer on nanoparticles of other metals[19] have been synthesized in narrow particle size distribution.

The polymer electrolyte fuel cell (PEFC) is expected to be a portable and compact power source to start at atmospheric temperature and be operated at lower than 373 K for automobile and home use.[20] In the design of PEFCs, the cathode catalyst for the oxygen reduction reaction ($O_2 + 4H^+ + 4e^- \rightarrow 2H_2O$) is most critical because the physical contact of Pt with C (electric contact), the electrolyte (wet polymer to transport protons), and oxygen gas needs to be enabled at the same time.[1] The morphologic effects of Pt nanoparticles, films, and alloys on the oxygen reduction reaction were reported.[1,21] In contrast that the Pt nanoparticles have been formed on various types of controlled C materials,[3–17] the electric contact of Pt with C has never been controlled and monitored nanoscopically.

In this work, the contact of Pt with C was controlled based on the idea of catalytic

acetylene decomposition over Pt nanoparticles in a narrow size distribution centered at 1.2 nm formed inside of Al-exchanged ordered mesoporous silica Al-MCM-41 to produce Pt-C composites in mesopores. The replica Pt-C composite was separated via the removal of Al-MCM-41 using hydrofluoric acid. The synthesis of the replica Pt-C composite was monitored using high-resolution transmission electron microscope (TEM), X-ray diffraction (XRD), and Brunauer, Emmett, and Teller (BET) adsorption of N_2. The local structure and heterogeneity of Pt sites were analyzed based on conventional Pt L_3- and L_2-edge X-ray absorption fine structure (XAFS) and state-selective Pt Lβ_1-selecting Pt L_2-edge XAFS, respectively. State-selective XAFS was applied to Pt catalysts for the first time.

The Pt nanoparticles in a narrow size distribution centered at 1.2 nm are advantageous to use most of the Pt sites (80%) for oxygen reduction;[1] however, mass-specific activity for oxygen reduction is still under debate and/or critically depends on reaction conditions. The rate constant values were nearly constant for mean Pt particles between 1.6 and 4.8 nm on C.[17] The mass-specific activity gradually decreased when the mean Pt particle size decreased from 30 to 1 nm[22] or reached a maximum at 3.5 nm.[23] The instability of Pt particles as small as 1 nm was suggested to be transformed into amorphous and less active.[9] In this paper, stabilization of Pt nanoparticles (mean 1.2 nm) was tried on/in a C matrix catalytically formed from acetylene in mesoporous space. The electronic structure of the interface Pt site between Pt nanoparticles and C was investigated. The replica Pt-C was pressed as a tentative cathode catalyst of membrane electrolyte assembly (MEA).

2.2 Syntesis of Replica Pt–C composite

Ten milliliters of an 8.4 mM aqueous solution of tetraammineplatinum(II) hydroxide hydrate $Pt^{II}(NH_3)_4(OH)_2 \cdot 2H_2O$ (Strem Chemicals) and 1.0 g of Al-MCM-41 (molar ratio SiO_2/Al_2O_3 = 0.9875/0.0125, 1.11 wt % Al; Aldrich) were mixed and stirred at 353 K for 2 days. The suspension was filtered, washed, and heated in vacuum at 573 K for 2 h. The obtained powder (Pt-Al-MCM-41, 1.3 wt % Pt) was in a 30 mL min^{-1} H_2 (>99.99%; 101 kPa) flow at 573 K for 2 h and then in a 200 mL min^{-1} C_2H_2 (>98%) + N_2 (>99.999%) flow (molar ratio 1:9, total 101 kPa) at 973 K for 1 h. The obtained black powder (0.72 wt % Pt) was treated with 30 mL of hydrofluoric acid (15%; special grade, Wako Pure Chemical) to give the replica Pt-C composite (0.84 wt % Pt). Fortunately, in view of electric conductivity, amorphous C dissolved in hydrofluoric acid, and Pt-graphite was preferably obtained.[6,24] Somanathan et al. prepared Pt nanoparticles starting from hydrogen hexachloroplatinate(IV) in Al-MCM (molar ratio SiO_2/Al_2O_3 = 0.995/0.005) followed by calcination at 823 K. In 200 mL min^{-1} of C_2H_2 + N_2 flow (molar ratio 3:7), the start of C decomposition at 923 K, carbon nanotube formation between 973 and 1073 K, the maximum C decomposed at 1073 K, and preferable formation of graphitic sheets and amorphous C at 1173 K were reported.[6] The starting temperature of C decomposition and the maximum decomposed C yield were reproduced in this work, but we chose a relatively low temperature of 973 K for C_2H_2 decomposition to prevent the thermal growth of Pt nanoparticles.

Replica Pt-C powder (76 mg) was dispersed in 1.0 mL of 15% Nafion dispersion solution (DE2021-CS, Wako Pure Chemical) using ultrasonic treatment (85 W, 28 kHz) and was mounted on 190 μm thick C paper coated with polytetrafluoroethylene (TGP-H-060H, Chemix). Similarly, 25 mg of commercial 20 wt % Pt supported on C

(Vulcan XC-72, Cabot) was dispersed on TGP-H-060H using a 5-10% Nafion dispersion solution. As a reference, mechanically dispersed Pt/Vulcan XC-72 on TGP-H-060H was also prepared. A 50 μm thick electrolyte polymer Nafion film (NR-212, Dupont; >95%; acid capacity > 9.2×10^{-4} equiv g^{-1}) was pressed with replica Pt-C/TGP-H-060H as the cathode and 20 wt % Pt/Vulcan XC-72/TGP-H-060H as the anode for MEA. Another MEA was made using the same Nafion film pressed with 20 wt % Pt/Vulcan XC-72/TGP-H-060H on both sides. The area of the electrode catalysts was 5 cm^2.

2.3 Physical properties for Replica Pt–C composite

Nitrogen adsorption measurements were performed at 77 K with the pressures between 1.0 and 90 kPa in a vacuum system connected to diffusion and rotary pumps (10^{-6} Pa) and equipped with a capacitance manometer (models CCMT-1000A and GM-2001, ULVAC). The samples were evacuated at 393 K for 2 h before measurements. Highresolution TEM images were taken using LaB_6 source TEM equipment (JEOL, Model JEM-4000FX) with an accelerating voltage of 400 kV. Samples were dispersed in ethanol (>99.5%, Wako Pure Chemical) and mounted on amorphous C-coated copper mesh (CU150 Mesh, JEOL).

XRD data were obtained using a Rigaku MiniFlex diffractometer at a Bragg angle of $2\theta_B$) 2-10° for ordered mesopores and 10-75° for crystallites of C and Pt. The conditions involved were 30 kV and 15 mA, Cu Kα emission, and a nickel filter. The replica Pt-C powder and each intermediate composite during the synthesis were set in a dip of $18 \times 2 \times 1$ mm^3 on glass plate to measure the electric conductivity with the twopoint method.[25]

2.4 Conventional Pt L_3-edge XAFS measurements

The powder samples for synchrotron X-ray measurements were prepared in the vacuum system (10^{-6} Pa) and transferred in situ to a Pyrex glass cell equipped with 25-50 μm thick Kapton (Dupont) windows on both sides. The samples in H_2, air, or argon were sealed with fire and transported to the beamline. The replica Pt-C powder was mounted on TGP-H-060H, as described above, but pressed to only one side of Nafion (NR-212) for synchrotron X-ray study. The Nafion and protection polyester films (50 μm) were used as a window of Pyrex glass cells.

Conventional Pt L_3- and L_2-edge XAFS spectra were measured at 290 K in transmission mode in the Photon Factory at the High-Energy Accelerator Research Organization (Tsukuba, Japan) on beamlines 9C and 12C. The storage-ring energy was 2.5 GeV, and the ring current was between 450 and 250 mA. A Si(111) double-crystal monochromator and cylindrical double mirror were inserted into the X-ray beam path. The parallelness of the double crystals was set to 65% intensity and to the maximum flux using a piezo translator. The slit opening size was 1 mm × 1 mm in front of the I_0 ionization chamber. The I_0 and I_t ionization chambers were purged with the mixture of Ar(15%) + N_2(85%) and Ar, respectively. The scan steps were ~7.8, ~0.46, and ~2.5 eV in the pre-edge, edge, and postedge regions, respectively. The accumulation time was 1-10 s for a data point. The Pt L_3- and L_2 absorption edge energy values were calibrated to 11562 and 13272.3 eV, respectively, for the spectra of Pt metal.[26,27]

2.5 State-selective Pt L_2-edge XAFS measurements

State-selective Pt L_2-edge XAFS measurements were performed at 290 K at the

beamline 37XU of SPring-8 (Sayo, Japan). The storage ring energy was 8 GeV at the top-up ring current of 100 mA. A Si(111) monochromator and rhodiumcoated mirror were used. The undulator gap was optimized to maximize the X-ray beam flux at each data point. To stabilize the X-ray beam position on the surface of the sample, the monochromator stabilization mechanism was used.[28]

The Pt Lβ_1 emission spectra were measured using a homemade Rowland-type fluorescence spectrometer set at beamline 37XU (Figure 2-1).[28–30] A Johann-type spherically bent Ge(844) crystal (Saint-Gobain; curvature radius of 450 mm, d = 0.57737 Å) and NaI(Tl) scintillation counter (SC; Model SP-10, Oken) were mounted. The energy resolution of the fluorescence spectrometer was estimated to be 3.4 eV at Pt L1, including the contribution of the beamline. The apparent core-hole lifetime width for Pt Lβ_1-selecting XAFS was estimated to be 2.0 eV based on the formula[31]

$$\frac{1}{\Gamma_{App}^{\ 2}} = \frac{1}{\Gamma_{Pt\ 3d_{3/2}}^{\ 2}} + \frac{1}{\Gamma_{Pt\ 2p_{1/2}}^{\ 2}}$$

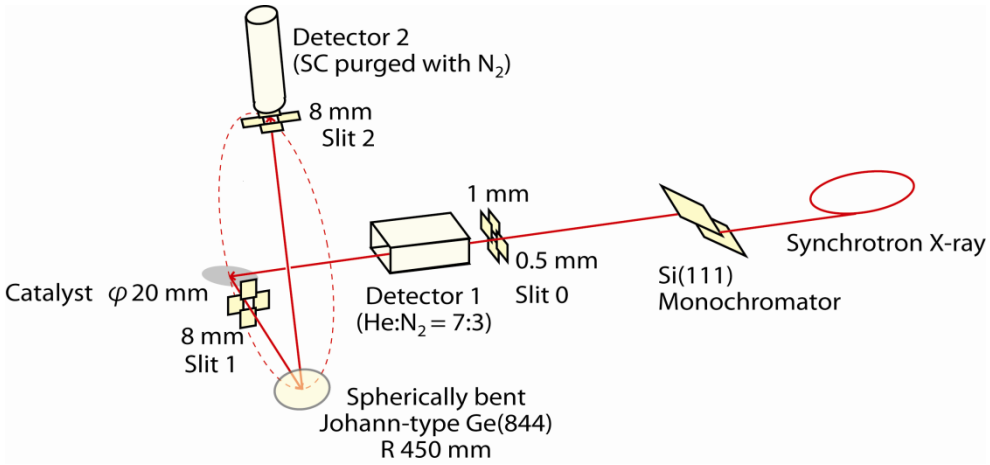

Figure 2-1. State-selective XAFS measurement set-up utilizing Rowland-type fluorescence spectrometer.

The gas for the ion chamber was 30% N_2 and 70% He in front of the sample. The slit opening in the front of the ionization chamber was 0.3 mm (horizontal) × 1.0 mm (vertical). The sample was placed in a plane near horizontal, tilted by 6° toward the incident X-ray and by 7° toward the Ge crystal. The sample surface, Ge crystal, and slit in front of the SC were controlled on a Rowland circle (radius 225 mm) in the vertical plane. The openings of the receiving slit and the slit in front of the SC were 8.0 mm (h) × 0.1 mm (v). The sample and SC were covered with a lead plate housing, except for the X-ray paths.

With the excitation energy set to 13298.8 eV, Pt Lβ_1 emission ($M_4 \rightarrow L_2$; θ_B) 75.895°) spectra were measured. The scan step was ~0.58 eV, and the accumulation time was 60 s for a data point. The fluorescence spectrometer was tuned to each energy around the Pt Lβ_1 emission peak, and Pt L_2-edge XANES (X-ray absorption near edge structure) spectra were measured. The scan step was ~0.46 eV with an accumulation time of 40-60 s for a data point. The Pt Lβ_1 fluorescence energy value was calibrated to 11070.84 eV for the spectrum of Pt metal.[26,27] The energy positions of the monochromator and the fluorescence spectrometer were reproduced within ±0.1 and ±0.2 eV, respectively.

2.6 XAFS data analysis

The XAFS data were analyzed with XDAP (XAFS Services International).[32] The pre-edge background was approximated by a modified Victoreen function $C_2/E^2 + C_1/E + C_0$. The background of the postedge oscillation was approximated by a smoothing spline function, calculated by an equation for the number of data points where k was the wavenumber of photoelectrons.

$$\sum_{i=1}^{\text{Data\_Points}} \frac{(\mu x_i - BG_i)^2}{\exp\left(-0.075 k_i^2\right)} \leq \text{ smoothing factor}$$

Multiple shell curve fit analyses were performed for the Fourier-filtered k^3-weighted EXAFS data in k and R space using empirical amplitude and phase shift parameters extracted from EXAFS of PtO_2 and Pt metal for Pt-O [bond distance R(Pt-O) = 0.1993 nm with the coordination number (N) of 6][33] and Pt-Pt bonds [R(Pt-Pt) = 0.2775 nm with the N of 12][4] based on reported crystal structures. The many-body reduction factor S_0^2 was assumed to be equal for the sample and reference. The goodness of fit was given as requested by the Committee on Standards and Criteria in X-ray Absorption Spectroscopy.

The Pt L_3- and L_2-edge XANES spectra were theoretically generated using ab initio calculation code FEFF 8.4,[34] operated in a self-consistent field and full multiple scattering modes. Theoretical calculations of Pt XANES were reported to clarify the Pt cluster size effect and spectral change upon H/CO adsorption.[35–37] The exchange-correlation potential of Hedin-Lundqvist was chosen and corrected by adding a constant shift of +1.0 eV to the Fermi level. The calculated potential was also corrected by adding a constant shift of -1.6 eV to the "pure imaginary optical potential" to compare to Pt Lβ_1-selecting Pt L_2-edge spectra, but no shift was given for comparison to conventional XANES. The energy of the theoretically generated spectrum was shifted by +4.7 eV to compare to conventional Pt $L_{3/2}$-edge spectra and Pt L_2-edge spectra tuned to the Pt Lβ_1 peak top (11070.7-11070.8 eV). Corresponding to the Pt L_2-edge spectra tuned to 11065.7 and 11075.4 eV, the energies of the theoretically generated spectra were shifted by 0 and +8.2 eV, respectively.

The Pt metal site model consisted of 38 atoms of a facecentered cubic (fcc) Pt metal cuboctahedron. Among the Pt atoms, *N*(Pt-Pt) values of 6, 8, and 24 atoms were 12, 9, and 6, respectively.[38] The central Pt atom in the (111) surface (N = 9) was considered as a representative Pt site for calculations (Figure 2-2) compared to an average N of 7.6 for all of the Pt sites. A central Pt atom in the (111) surface was in vacuum or at the interface with 177 atoms of three layers of graphite [R(C-C) = 0.1418 nm]. The Pt-C bond length was varied between 0.16 and 0.22 nm based on the crystal structures of organometallic compounds.[39] Relatively long R(Pt-C) values of 0.320-0.359 nm were used in the calculation model of Pt_{37} on graphite.[40] The Pt L_2-edge spectrum tuned to 11065.7 eV for replica Pt-C/Nafion was best reproduced theoretically by setting the R(Pt-C) to 0.18 nm. Thus, the nearest Pt-C bond distance was fixed to 0.18 nm. Average R(Pt-C) and N values were 2.0 nm and 1.9, respectively, for seven Pt atoms at the interface (Figure 2-2).

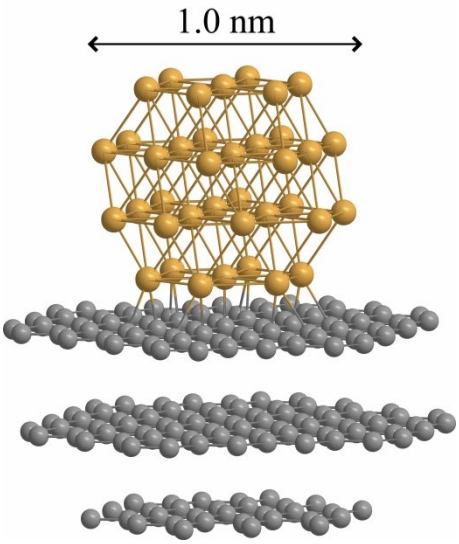

Figure 2-2. The Pt_{38} cluster model on three layers of graphite for XAFS analyses.

2.7 Fuel cell tests

A PEFC single cell (Model EFC-05-02, Electrochem) was used for evaluation of replica-Pt-C as cathode catalyst at 343 K. The H2 (> 99.99%, CO < 0.1 ppm) and dried air were flowed through anode and cathode, respectively, both with the flow rates of 100 mL min^{-1}. Water bubble via ball filter with aperture size 5 – 10 μm was inserted in the H_2 flow path at 15 cm to the inlet to anode. The temperature of water, FC, and the gas flow path between water bubble and FC was controlled at 343 K using water bath and ribbon heater.

2.8 Results

2.8.1 N_2 adsorption, XRD, TEM, and conductivity

The specific surface area (S_{BET}) of 970 m^2 g^{-1} for Al-MCM-41 decreased by 21% upon impregnation of Pt (Table 2-1). In contrast to this partial block of mesopores, the S_{BET} for Pt-Al-MCM-41 decreased by 95% after catalytic C_2H_2 decomposition, suggesting that a (nearly) complete block of mesopores by C formed. The loss of S_{BET} was recovered to 540 m^2 g^{-1} with the HF treatment (Table 2-1).

The regularity of MCM-41 framework was monitored by XRD during the synthetic step of replica-Pt-C. The distance between pore and neighboring pore (a_0 of unit cell) was 4.7 nm (d_{100} = 4.1 nm) for Al-MCM-41 (Table 1).[6,41] The value decreased to 4.5 nm (d_{100} = 3.9 nm) upon impregnation of Pt, in similar trend to Ref. [6]. In contrast, no peak was detected in XRD for Pt-C-Al-MCM-41 probably because the electron density of C formed in Al-MCM-41 mesopores was similar to that of Al-SiO_2 template. The lower angle peaks recovered at d = 3.7 and 3.2 nm for replica-Pt-C composite, but the intensity was weaker compared to peak for Pt-Al-MCM-41. No distinct peaks

Table 2-1: Physicochemical Characterization of Intermediate and Final Materials in the Replica-Pt-C Composite Synthesis

	Specific	Pt				TEM[d]	XRD[e]	Electric	
	S_{BET}	$R_{Pore-Pore}$	loading		N_{Pt-O}	d_{Pt-Pt}		conductivity	
Sample	(m^2 g^{-1})	(nm)[a]	(wt%)[b]	N_{Pt-Pt}[c]	or N_{Pt-C}[c]	(nm)		(mS cm^{-1})	Ref.
Al-MCM-41	970	4.7	—	—	—	—		< 0.001	this work
Pt-Al-MCM-41	767	4.5	1.3	—	—	—		< 0.001	this work
Pt-C-Al-MCM-41 35	n.p.[f]	0.72	5.1	2.1	—	n.p.[f]	263		this work
Replica-Pt-C	540	—	0.84	6.1	2.2	1.2	n.p.,[f] n.p.[f,g]	259	this work
Pt/Vulcan XC-72	—	—	20	12	—	—	4.8	224	this work
Hexagonal Pt-Block copolymer composite	18	30	74					2.5	25

[a] Distance from center of pore to center of neighboring pore based on XRD. [b] Based on Pt L_3-edge jump value. [c] Coordination number based on Pt L_3-edge EXAFS curve fit analysis. [d,e] Average particle size of Pt based on TEM images[d] or XRD[e]. [f] No peak detected. [g] Sample after PEFC cell test for 3 h.

derived from Pt or C crystalline were observed throughout the synthetic step of replica-Pt-C. After fuel cell test for 3 h, the replica-Pt-C composite used as cathode was re-examined by XRD. No peak was observed in the range of $2\theta_B$ = 10 – 75°, suggesting the Pt particle size remained small.

TEM image for replica-Pt-C was depicted in Figure 2-3A. Darker dots of Pt particles were clearly observed between 0.38 and 3.33 nm (Figure 2-3C). The mean particle size was 1.2 nm with the standard deviation 0.5 nm. The mean size corresponds to total 66 atoms in one particle.[38] Most of the Pt particles were within the pore size of Al-MCM-41 (2.7 nm) (Figure 2-3C). The replica-C was not clear in TEM images probably because the axis of replica-Pt-C may randomly distribute and the diameter of the rod/tube-like structure should be less than 3 nm dispersed over amorphous C coated on Cu mesh. However, the straight arrangement of darker Pt spots was observed, reminiscent of ordered mesoporous structure of Al-MCM-41 framework (Figure 2-3B).

The electric conductivity for Pt-Al-MCM-41 less than 1 μS cm^{-1} dramatically increased to 263 mS cm^{-1} upon catalytic C_2H_2 decomposition (Table 2-1). The value was by 17% superior to that for 20 wt% Pt/Vulcan XC-72. The value for replica-Pt-C (259 mS cm^{-1}) was comparable to that for Pt-C-Al-MCM-41 (Table 2-1).

2.8.2 Conventional XANES

Conventional Pt L_3-edge XANES spectra were measured during synthetic steps of replica-Pt-C composite (Figure 2-4). The peak positions of XANES for Pt-Al-MCM-41 (11565.7, 11580.5, and 11594.2 eV; spectrum a) were similar to those for Pt metal (spectrum e). The intensity of three post-edge peaks was weaker for

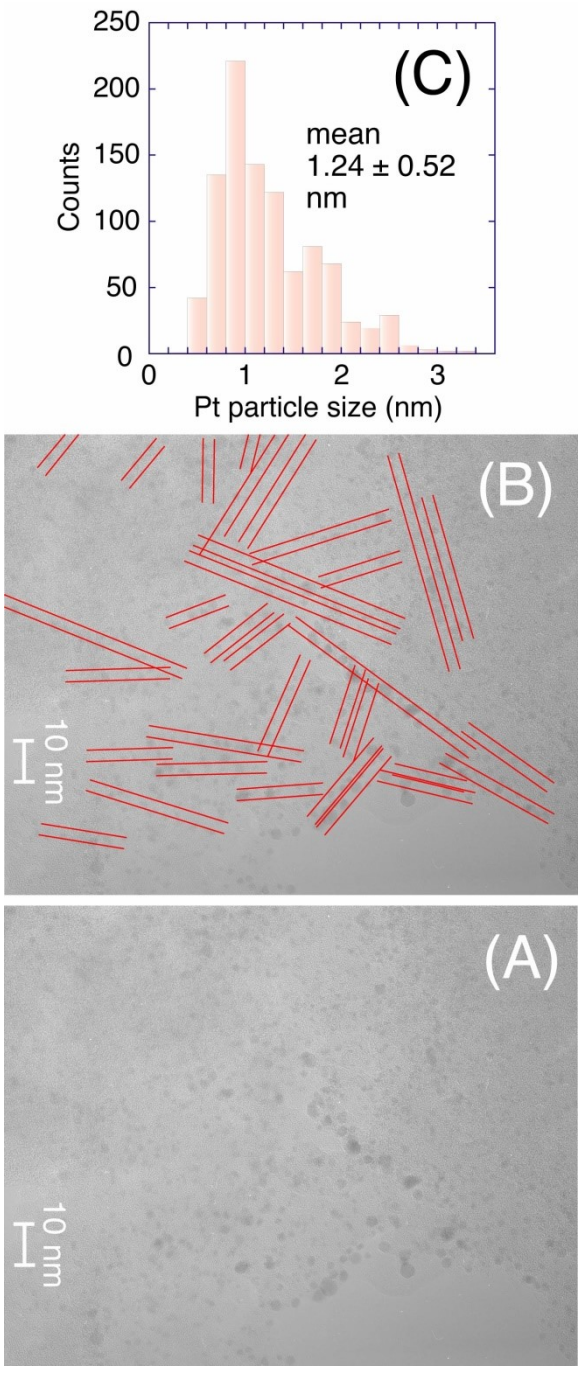

Figure 2-3. High-resolution TEM image for replica-Pt-C (A). The internal size of mesopores of Al-MCM-41 was added in (B). The size distribution of darker dots of Pt particles (C).

Pt-Al-MCM-41 compared to those of corresponding peaks for Pt metal, demonstrating that the Pt particles in Pt-Al-MCM-41 were on nanometer scale.

The peak at 11566.5 eV for Pt-C-Al-MCM-41 (spectrum b) became weaker and broader compared to that at 11565.7 eV in spectrum a. The spectra a and b were tried to be fit with theoretical spectra for metallic Pt site or interface Pt site between metal and graphite. It was difficult to fit because spectrum a seemed to be the mixture for metallic and oxidic Pt sites. Spectrum b seemed to be the mixture for metallic Pt and Pt at the interface with C. Instead, Pt $L\beta_1$-selecting XANES spectra were compared to theoretical data because the Pt state was selected and spectral pattern was sharpened.[28,29,42–47]

The XANES spectrum for replica-Pt-C composite in air was shown in Figure 2-4c. The energy of first peak above the absorption edge (11566.7 eV) was intermediate

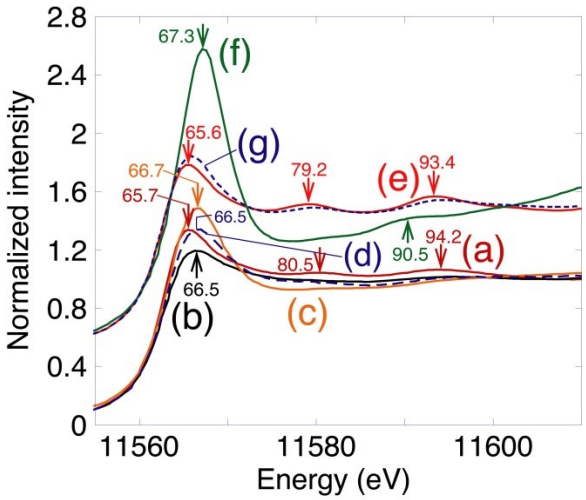

Figure 2-4. Normalized Pt L_3-edge XANES spectra for Pt-Al-MCM-41 (a), Pt-C-Al-MCM-41 (b), replica-Pt-C in air (c), replica-Pt-C/Nafion in air (d), Pt metal of 5 μm thickness (e), PtO_2 (f), and 20 wt% Pt/Vulcan XC-72/Nafion (g).

between peak at 11565.6 eV for Pt metal (spectrum e) and one at 11567.3 eV for PtO_2 (spectrum f). The first peak for spectrum c was more intense (1.47) than those for spectra a, b (1.33 – 1.19) and post-edge pattern of spectrum c became featureless. Thus, oxidation of part of metallic Pt in Pt-C-Al-MCM-41 was suggested after the removal of Al-MCM-41 framework. In the XANES spectrum for Pt sites in replica-Pt-C/Nafion in air (Figure 2-4d), the first peak above the absorption edge shifted down to 11566.5 eV and the intensity decreased (1.34). The peak intensity was essentially identical to that for spectrum a (1.34 *v.s.* 1.33). No peak feature at 11590.5 eV for PtO_2 (spectrum f) was detected in spectrum d. The post-edge pattern of spectrum d was most alike that of spectrum b.

In comparison, XANES pattern of 20 wt% Pt/Vulcan XC-72/Nafion (Figure 3g) corresponded exactly to that for Pt metal (spectrum e). The mean Pt particle size in the sample was 4.8 nm based on the peak width of XRD, much greater than that in replica-Pt-C composite (1.2 nm) and less effectively in contact with Nafion.

2.8.3 X-ray Emission and State-Selective XANES

The Pt $L\beta_1$ emission peaks for replica-Pt-C/Nafion in H_2 or in air appeared at 11070.7 – 11070.8 eV (Figure 2-5c, d), essentially identical to that for Pt metal (11070.84 eV). The emission peak for replica-Pt-C powder in air was 11071.0 eV (spectrum b), shifted by +0.2 eV from that for Pt metal. The FWHM (full width at the half maximum) values were relatively greater (7.5 – 7.6 eV) for replica-Pt-C/Nafion and replica-Pt-C powder compared to 7.1 – 7.2 eV for standard Pt compounds and 20 wt% Pt/Vulcan XC-72/Nafion (spectrum a).

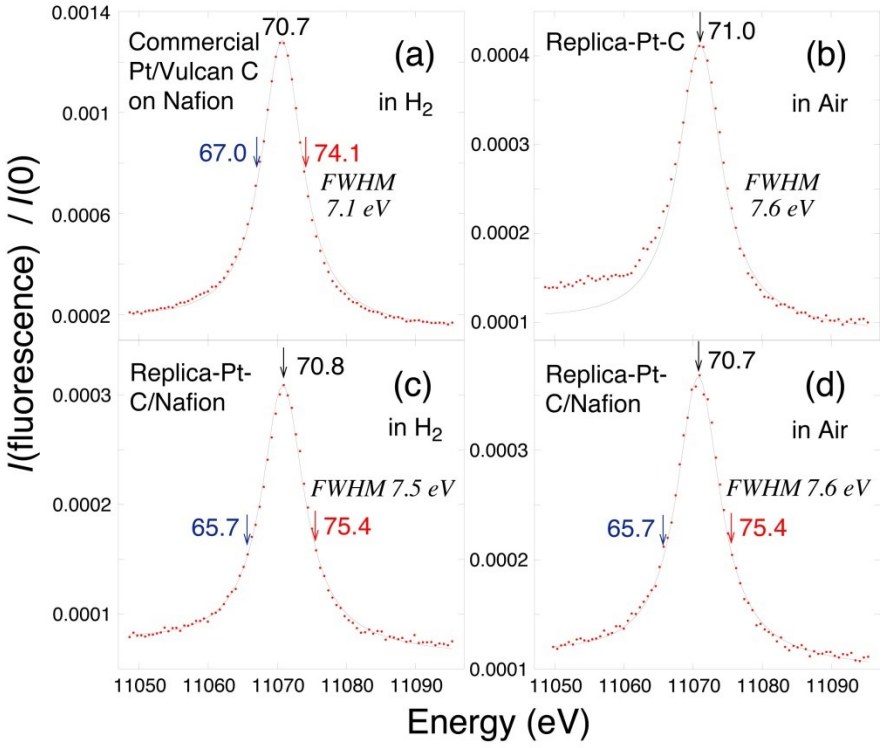

Figure 2-5. Pt $L\beta_1$ emission spectra for Pt/Vulcan XC-72/Nafion in H_2 (a), replica-Pt-C in air (b), replica-Pt-C/Nafion in H_2 (c), and replica-Pt-C/Nafion in air (d). The arrows indicate tune energy values for Pt $L\beta_1$-selecting XAFS measurements (Figure 2-6).

Then, Pt L_2-edge XANES spectra were measured (Figure 2-6B) tuned to Pt $L\beta_1$ peak top (11070.7 – 11071.0 eV, the arrows in Figure 2-5). The absorption edge position progressively shifted from 13272.3 eV for Pt metal (spectrum a), to 13272.8 eV for replica-Pt-C/Nafion in H_2 (spectrum f), 13272.9 eV for replica-Pt-C/Nafion in air (spectrum e), 13273.4 eV for replica-Pt-C in air (spectrum d), then to 13274.2 eV (PtO_2, spectrum b). In spite of the gradual edge shift, post-edge peaks appeared at almost the same position (13287 – 13289, 13302, 13312, and 13327 eV) for replica-Pt-C/Nafion in H_2/in air and replica-Pt-C in air (spectra d – f) as those for Pt metal (spectrum a).

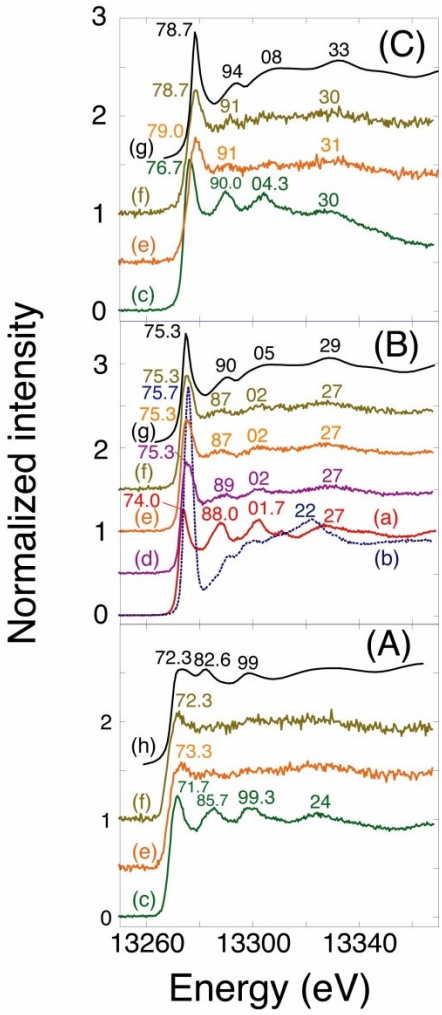

Figure 2-6. Normalized Pt L_2-edge XANES spectra for Pt metal (a), PtO_2 (b), 20 wt% Pt/Vulcan XC-72/Nafion in H_2 (c), replica-Pt-C in air (d), replica-Pt-C/Nafion in air (e), and replica-Pt-C/Nafion in H_2 (f). The tune energy was 11067.0 eV (c) and 11065.7 eV (e, f) in panel A, 11070.8 eV (a), 11070.6 eV (b), 11071.0 eV (d), 11070.7 eV (e), and 11070.8 eV (f) in panel B, and 11074.1 eV (c) and 11075.4 eV (e, f) in panel C (see the arrows in Figure 2-5). Theoretically generated Pt L_2-edge XANES spectrum for central Pt atom in (111) face of cubo-octahedral Pt_{38} cluster (g) and the atom in contact with graphite layers [R(Pt–C) = 0.18 nm, R(C–C) = 0.1418 nm] (h). The energy shifts were 0, 4.7, and 8.2 eV for spectrum A-h, B-g, and C-g, respectively.

Thus, metallic Pt states were selected in replica-Pt-C samples (as powder or on Nafion) in XANES spectra tuned to 11070.7 – 11071.0 eV.

Pt L_2-edge XANES spectra tuned to lower energy side of Pt $L\beta_1$ peaks (11065.7 – 11067.0 eV, the arrows in Figure 2-5) were shown in Figure 2-6A. The first intense peak at 13272.3 – 13273.3 eV above the absorption edge (spectra 2-6A-e, f) became weaker compared to the peaks in spectra tuned to Pt $L\beta_1$ peak top (panel B-e, f). The absorption edge position for replica-Pt-C/Nafion shifted from 13267.9 eV in H_2 to 13268.1 eV in air.

The post-edge pattern for 20 wt% Pt/Vulcan XC-72/Nafion (spectrum 2-6A-c) resembled that of metallic Pt tuned to Pt $L\beta_1$ peak top (Figure 2-6B-a) if the spectrum 2-6B-a shifted by 2.3 eV toward lower energy side. In contrast, the post-edge pattern of spectra 2-6A-e and f for replica-Pt-C/Nafion became featureless in panel A and did not resemble that of metallic Pt nor PtO_2. The spectra e and f resembled theoretical spectrum for the interface Pt atom between Pt metal and graphite (Figures 2-2 and 2-6A-h) when the energy was shifted by –4.7 eV relative to XANES tuned to Pt $L\beta_1$ peak top.

Next, Pt L_2-edge XANES spectra tuned to higher energy side of Pt $L\beta_1$ peaks (11074.1 – 11075.4 eV, the arrows in Figure 2-5) were measured for replica-Pt-C/Nafion compared to 20 wt% Pt/Vulcan XC-72/Nafion (Figure 2-6C). The post-edge pattern for spectra 5C-e and f resembled that of corresponding spectra tuned to Pt $L\beta_1$ peak top (Figure 2-6B-e, f) if the spectra 2-6B-e and f shifted by 3.5 eV toward higher energy side. The spectra e and f resembled theoretical spectrum for Pt atom in Pt nanoparticle (Figure 2-6C-g) when the energy was shifted by +3.5 eV relative to XANES tuned to Pt $L\beta_1$ peak top (Figure 2-6B-g). The absorption edge position for replica-Pt-C/Nafion in

air (13276.4 eV) was by 1.0 eV greater than that in H_2. Post-edge peak shifts were within 1 eV toward higher energy side by switching the ambient gas from H_2 (spectrum f) to air (spectrum e).

The post-edge pattern for 20 wt% Pt/Vulcan XC-72/Nafion (spectrum 2-6C-c) resembled that of metallic Pt tuned to Pt $L\beta_1$ peak top (Figure 2-6B-a) if the spectrum 5B-a shifted by 2.7 eV toward higher energy side. The Pt $L\beta_1$ tune energy for spectrum C-c was greater by 3.4 eV compared to peak top. The Pt $L\beta_1$ tune energy for spectrum A-c was smaller by 3.7 eV compared to peak top and the XANES peaks shift was 2.3 eV. The reduction of tune energy difference *v.s.* XAFS energy difference was 62 – 80% mainly due to final state relaxation effect.[48]

2.8.4 Catalyst performance in PEFC

The catalytic performance of replica-Pt-C composite was compared to that of conventional 20 wt% Pt/Vulcan XC-72 as cathode in PEFC. In the *I-V* plots per electrode area (Figure 2-7A), the current density using replica-Pt-C (data a and b) was by 35% greater at maximum than that using 20 wt% Pt/Vulcan XC-72 (data c). The difference between curves a and b was due to the press conditions for MEA. Nafion solution (5 – 15%) was used to disperse replica-Pt-C or 20 wt% Pt/Vulcan XC-72 on TGP-H-060H before the press to make MEA for curves b and c, whereas mechanically dispersed Pt/Vulcan XC-72 on TGP-H-060H was directly pressed as MEA for curve a. The current density for curve a extended greater in which the 50-μm Nafion film and anode 20 wt% Pt/Vulcan XC-72 constituted better interface without excess Nafion added (curve a).

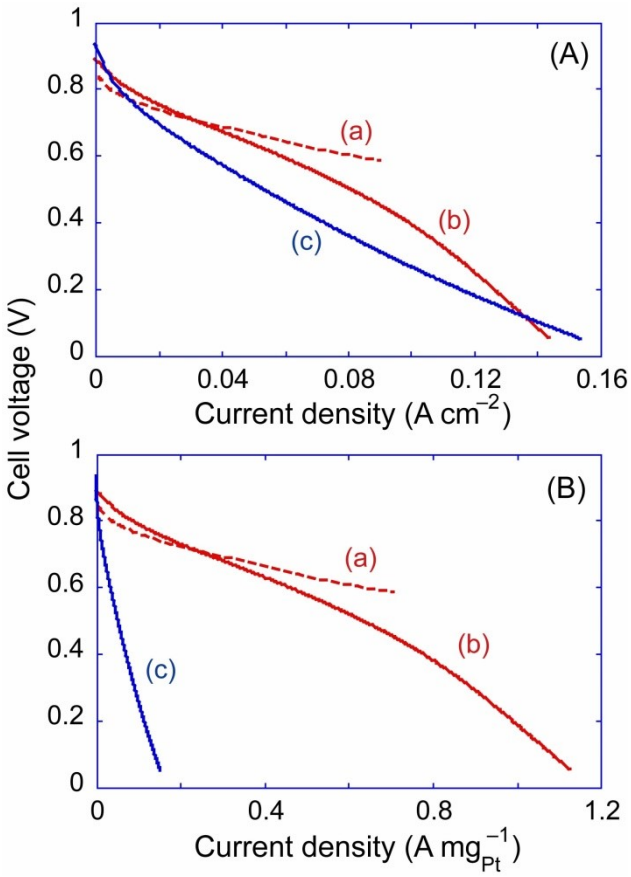

Figure 2-7. Dependence of cell voltage as a function of current density per electrode area (A) and per Pt weight (B) for H_2-air PEFC with replica-Pt-C (cathode) and 20 wt% Pt/Vulcan XC-72 (anode) (a, b) and with 20 wt% Pt/Vulcan XC-72 (cathode, anode) (c). The temperature of water bubble, FC, and H_2 flow path in between was controlled at 343 K.

The inflection point for curve b at 0.10 A cm^{-2} should be due to the lack of fuel gas because of the balance of activity and Pt amount. The Pt amount per electrode area was 0.13 mg-Pt cm^{-2} *versus* 1 mg-Pt cm^{-2} for conventional 20 wt% Pt/Vulcan XC-72. Therefore, the *I-V* plots were redrawn per Pt amount in cathode (Figure 2-7B). The current density using replica-Pt-C (curve a and b) was 12 times greater than that using

20 wt% Pt/Vulcan XC-72 (curve c) below the inflection point at 0.77 A mg-Pt^{-1}. The current density per Pt amount was 1.08 and 0.14 A mg-Pt^{-1} for H_2-air PEFC with replica-Pt-C as cathode and for 20 wt% Pt/Vulcan XC-72 as cathode, respectively, at the cell voltage of 0.1 V. The current density for commercial Pt/C was relatively low (Figure 2-7B-c)[49] probably because the MEA press condition was not optimized in this work. Note that the press condition of samples for curves b and c was nearly identical for comparison of PEFC tests.

The surface dispersion of Pt atoms needs to be taken into account to evaluate turnover number. The mean Pt particle sizes of 1.2 and 4.8 nm (Table 2-1) correspond to Pt surface dispersion of 0.8 and 0.3, respectively. Thus, the current density values corresponded to turnover numbers of 2.8 and 0.9 s^{-1}, respectively. The reason of this 3 times improvement was intimate contact of Pt with C matrix catalytically grown from C_2H_2. The quicker O_2 gas diffusion in cathode may also affect because the diameter of replica-C rod/tube should be smaller than 2.7 nm of ordered pores of Al-MCM-41 in comparison to conventional C particles of 0.1 – 1 μm.[14–17,22,23]

The possibility to reduce the Pt nanoparticle size to 1.2 nm keeping the metallic reactivity was demonstrated stabilized on/in the C matrix catalytically produced over the Pt nanoparticles, in clear contrast to structural instability of Pt[9,17] and activity decrease for oxygen reduction for Pt particles less than 3.5 nm.[22,23]

2.9 Discussions

2.9.1 Replica-Pt-C Morphology

The Pt loading in Pt-Al-MCM-41 was 1.3 wt% after cation exchange and reduction in H_2 at 573 K (Table 2-1). The amount corresponds to 67.5 μmol of Pt substituting on the proton sites for 1 g of Al-MCM-41 (412 μmol-Al g^{-1}). Therefore, 32.8% (or

16.4%) of proton sites of Al-MCM-41 were exchanged to $[Pt(NH_3)_4]^{2+}$ species (or $[Pt(NH_3)_4(OH)]^{+}$ species). This exchange ratio was greater than values for Pt-zeolites,[50] but the Pt amounts introduced in samples were similar between 0.6 and 2.0 wt% due to the difference of Al concentrations: 10 – 12 wt% for zeolites[50] *v.s.* 1.11 wt% for Al-MCM-41 of this work.

The Pt loading for Pt-C-Al-MCM-41 was 0.72 wt% after catalytic C_2H_2 decomposition at 973 K over Pt particles in Al-MCM-41 (Table 2-1). Therefore, C content in the Pt-C-Al-MCM-41 was 44.6%. If the pore volume for Al-MCM-41 was 0.6 $cm^3\ g^{-1}$,[41] the density of formed C was 2.25 g cm^{-3} (graphite), and catalytically formed C remained exclusively inside the mesopores of Al-MCM-41 (HR-TEM), it is estimated that 60.5% of the mesopores was stuffed. No C rod/tube pushed out of mesopores was detected in TEM images for Pt-C-Al-MCM-41 (not shown). The S_{BET} value for Pt-Al-MCM-41 (767 $m^2\ g^{-1}$) decreased by 95% after catalytic C_2H_2 decomposition (Table 2-1), supporting effective block of mesopores. Only external surface of Al-MCM-41 adsorbed N_2.

The Pt loading for replica-Pt-C was 0.84 wt% after the removal of Al-MCM-41 framework (Table 2-1). Therefore, 47.4% of Pt in Pt-C-Al-MCM-41 was lost during the washing with HF solution. The specific S_{BET} value for replica-Pt-C recovered as much as 540 $m^2\ g^{-1}$ (Table 2-1). When the catalytic C_2H_2 decomposition temperature was 1073 K, thermally decomposed C was formed as by-product, but can be separated from Pt-C-Al-MCM-41. The C content in the Pt-C-Al-MCM-41 was 66.0%. It is estimated that 143.9% of mesopores for Al-MCM-41 was stuffed, suggesting excessive C was pushed out of mesopores. At 873 K, acetylene did not react either catalytically or thermally in consistent with Ref. [6].

When catalytic C_2H_2 decomposition was performed at 973 K in closed circulation system or in batch for Pt-Al-MCM-41, the decomposition was by 75% slower than that in flow setup in this study. Formed H_2 due to C_2H_2 decomposition remained in the system and inhibited further C_2H_2 decomposition due to equilibrium. When MCM-41 or FSM-16 was used instead of Al-MCM-41, ion exchange was not applicable to introduce Pt species. Catalytic C_2H_2 decomposition was performed on the Pt nanoparticles, followed by HF treatment. The Pt content in obtained replica-Pt-C was only 0.09 wt%.

The mean Pt particle size was 1.2 nm for replica-Pt-C (Figure 2-3A, C). The average *N* value for Pt–Pt bonds by EXAFS (6.1; Table 2-1) suggested even smaller Pt nanoparticles.[38] This discrepancy is due to the contribution of $N_{Pt–O}$ or $N_{Pt–C}$. Pt-C-Al-MCM-41 and replica-Pt-C samples measured both in air provided $N_{Pt–O}$ values of 2.1 – 2.2 including the undividable contribution of $N_{Pt–C}$ (Table 2-1) because the exterior of these Pt nanoparticles should be oxidized and/or carburized.

2.9.2 Pt Sites in Replica-Pt-C

Partial oxidation of Pt sites was demonstrated in conventional Pt XANES for replica-Pt-C composite (Figure 2-4c). In contrast, high energy-resolution Pt L_2-edge XANES spectrum (Figure 2-6B-d) tuned to Pt $L\beta_1$ peak top (11071.0 eV; Figure 2-5b) preferably selected metallic Pt. The emission of Pt(IV) sites appeared at 11070.6 eV (not shown) and the spectral pattern tuned to 11070.6 eV for PtO_2 (Figure 2-6B-b) was totally different from spectrum d.

Conventional XANES for replica-Pt-C/Nafion (Figure 2-4d) was similar to that for Pt metal (spectrum e) in the absorption edge region or that for Pt-C-Al-MCM-41

(spectrum b) in the post-edge region. The XANES spectra tuned to Pt $L\beta_1$ peak top for replica-Pt-C/Nafion both in air or in H_2 exclusively detected metallic Pt sites (Figure 2-6B-e, f). The spectra resembled well theoretical spectrum 2-6B-g generated for surface Pt site in (111) face of cubo-octahedral Pt_{38} cluster.

When the tune energy was on the lower energy side of Pt $L\beta_1$ peak for replica-Pt-C/Nafion (Figure 2-5-c, d), the first intense peak at 13272.3 – 13273.3 eV became weaker (Figure 2-6A-e, f), suggesting greater occupation of Pt 5d band. The spectra e and f resembled well theoretical spectrum 2-6A-h calculated for interface site between Pt nanoparticle and graphite layers (Figure 2-1). Thus, interface Pt sites were predominantly selected in Pt L_2-edge XANES tuned to 11065.7 eV for replica-Pt-C/Nafion and negative charge transfer from C to Pt nanoparticles was suggested. However, the selective detection of interface Pt sites was unsuccessful for Pt(mean size 4.8 nm, Table 2-1)/Vulcan XC-72/Nafion. Only dominant metallic Pt sites appeared in XANES tuned to 11067.0 eV.

EXAFS in general provides statistical bonding information for Pt in sample irradiated with X-ray. Therefore, Pt–C bonds are statistically preferably detectable for the Pt sites in Pt particles in narrow size distribution centered at 1.2 nm compared to Pt sites in Pt particles of mean size 4.8 nm. Even so, the contribution of Pt–C bonds was statistically minor for replica-Pt-C compared to that of Pt–Pt bonds (Figure 2-4a, b). High energy-resolution XAFS in this work still provides statistical bonding information, however, the information was specific for Pt sites corresponding to lower Pt $L\beta_1$ emission energy 11065.7 eV for replica-Pt-C/Nafion (Figure 2-6A-e, f) and Pt/Vulcan XC-72/Nafion (Figure 2-6A-c). Thus, the discussion is reasonable that Pt sites in contact with C were discriminated among smaller Pt particles in replica-Pt-C/Nafion

and the XANES spectrum was compared to theoretical XANES data (Figure 2-6A-h) for the interface Pt sites depicted in Figure 2-2. Even tuned to lower Pt $L\beta_1$ energy 11067.0 eV, Pt–C interface site was not discriminated for Pt-Vulcan XC-72/Nafion because the site population was too small among Pt sites corresponding to lower Pt $L\beta_1$ emission energy. It is apparent that the reason was greater mean Pt particle size and predominant population of Pt–Pt bonds in Pt/Vulcan XC-72/Nafion.

The XANES spectra tuned on higher energy side of Pt $L\beta_1$ (Figure 2-5c, d) for replica-Pt-C/Nafion resembled theoretical spectrum 2-6C-g generated for surface Pt site in (111) face of Pt_{38}, shifted by +3.5 eV from spectrum 2-6B-g. This XANES shift was rationalized based on the difference of fluorescence tune energy and final state relaxation effect. Metallic Pt state was selected in the XANES tuned to 11075.4 eV.

Due to selection rule of electronic transition (azimuthal quantum number $\Delta l = \pm 1$, total angular momentum $\Delta j = 0, \pm 1$), the near-edge transition from L_2 ($^2P_{1/2}$) is limited to O_4 ($^2D_{3/2}$) at deeper energy than O_5 ($^2D_{5/2}$) whereas those from L_3 ($^2P_{3/2}$) are both to O_4 and O_5.[50] This is the reason why Pt L_2-edge white line is weaker than that in Pt L_3-edge spectra.[35] By changing the fluorescence tune energy between 11065.7 and 11075.4 eV (Figure 2-5c, d), electron-sufficient Pt sites in contact with C (Figure 2-6A-e, f) and relatively electron-deficient Pt sites on/in Pt nanoparticles (Figure 2-6B, C-e, f) were discriminated, respectively. In contrast, negligible difference was detected by switching the ambient gas from H_2 to air for replica-Pt-C/Nafion except for absorption edge shift less than 1 eV (Figure 2-6e, f). Shape resonance peak near L_3-edge was reported *e.g.* by H adsorption on Pt.[35,36,50] One of the possibilities is that anti-bonding level between Pt $5d_{3/2}$ and frontier level of adsorbent was occupied for replica-Pt-C/Nafion samples. It is also possible that similar shape resonance peak

appeared due to adsorbed H in H_2 and adsorbed O_2 in air. Technical reason may be that the XAFS measurements for Pt catalysts on Nafion were done as in half-cell and no water was supplied/catalytically produced in samples during the measurements. The contact of Pt with C(solid) and Nafion(liquid) was found to be secure, however, Nafion in pure H_2 or air was not entirely mobile and thus may block the Pt/gas interface sites.

2.9.3 Implications to PEFC Cathode Catalyst of Replica-Pt-C

The electric conductivity for Pt-C-Al-MCM-41 was by 17% superior to that for conventional 20 wt% Pt/Vulcan XC-72 (Table 2-1) probably because catalytically formed C in mesopores was regularly oriented in the [001] direction of Al-MCM-41 in spite of low Pt content in Pt-C-Al-MCM-41 (0.72 wt%). The comparable conductivity values for Pt-C-Al-MCM-41 and replica-Pt-C (Table 2-1) were also understandable if we think that non-conducting Al-MCM-41 part was removed but regular orientation of C rod/tube would be lost for the latter.

To enable 0.13 mg-Pt cm^{-2} as cathode catalyst, 76 mg of replica-Pt-C (0.84 wt% Pt) was mounted on C paper *versus* 25 mg of 20 wt% Pt/Vulcan XC-72 on C paper (1 mg-Pt cm^{-2}). The greater amount of replica-Pt-C mounted caused the difficulty to make physical contact of Pt with electrolyte (wet polymer to transport protons) and oxygen gas (fuel) at the same time.[1] Hence, to enable practical electric power generation using replica-Pt-C catalyst, Pt content in replica-Pt-C powder should be increased to 20 wt% Pt typical for other commercial Pt/C catalysts while keeping the Pt particle size of 1.2 nm. One possibility is to increase the Al content from 1.11 wt% to zeolite level 10 – 12 wt% to augment cationic Pt complexes exchanged. Another possibility is to utilize 3-dimensional mesoporous template, *e.g.* MCM-48, to stabilize

Pt nanoparticles on/in formed C in the 3-dimensional mesopores. The advantage to synthesize metal particles in narrow size distribution centered at ≈1 nm and secure contact of metal and C demonstrated in this paper can be applied to non-precious metal-C catalysts, *e.g.* cobalt or iron porphyrin decomposition[51] in mesoporous SiO_2-based templates. Carbonization of block copolymer self-assembled with Pt, Pb, and Nb species is another possibility to produce Pt-C composite as recently reported for anode material resistive to CO poisoning.[52]

2.10 References

[1] Gasteiger, H. A.; Markovic, N. M. *Science* **2009**, *324*(5923), 48 – 49.

[2] Zhang, G.; Yamaguchi, T.; Kawakami, H.; Suzuki, T. *Appl. Catal. B* **1992**, *1*(3), L15 – L20.

[3] Xuyen, N. T.; Jeong, H. K,; Kim, G.; So, K. P.; An, K. H.; Lee, Y. H. *J. Mater. Chem.* **2009**, *19*(9), 1283 – 1288.

[4] Plomp, A. J.; Schubert, T.; Storr, U.; de Jong, H. P.; Bitter, J. H. *Topics Catal.* **2009**, *52*(4), 424 – 430.

[5] Du, H. Y.; Wang, C. H.; Hsu, H. C.; Chang, S. T.; Chen, U. S.; Yen, S. C.; Chen, L. C.; Shih, H. C.; Chen, K. H. *Diamond Relat. Mater.* **2008**, *17*(4/5), 535 – 541.

[6] Somanathan, T.; Pandurangan, A. *J. Porous Mater.* **2009**, *16*(4), 459 – 464.

[7] Saha, M. S.; Li, R.; Ye, S. *Electrochem. Commun.* **2009**, *11*(2), 438 – 441.

[8] Chen, C.; Chen, M.; Yu, H.; Lu, S.; Chen, C. *Jpn. J. Appl. Phys.* **2008**, *47*(4), 2324 – 2329.

[9] Sun, Y.; Zhuang, L.; Lu, J.; Hong, X.; Liu, P. *J. Am. Chem. Soc.* **2007**, *129*(50), 15465 – 15467.

[10] Sun, C.; Chen, L.; Su, M.; Hong, L.; Chyan, O.; Hsu, C.; Chen, K.; Chang, T.; Chang, L. *Chem. Mater.* **2005**, *17*(14), 3749 – 3753.

[11] Hayashi, A.; Kitajima, K.; Miyamoto, J.; Yagi, I. *Chem. Lett.* **2009**, *38*(4), 346 – 347.

[12] Wikander, K.; Hungria, A. B.; Midgley, P. A.; Palmqvist, E. C.; Holmberg, K.; Thomas, J. M. *J. Colloid Interface Sci.* **2007**, *305*(1), 204 – 208.

[13] Joo, S. H., Choi, S. J.; Oh, I.; Kwak, J.; Liu, Z.; Terasaki, O.; Ryoo, R. *Nature* **2001**, *412*(6843), 169 – 172.

[14] Hui, C. L.; Li, X. G.; Hsing, I. M. *Electrochim. Acta* **2005**, *51*(4), 711 – 719.

[15] Prabhuram, J.; Wang, X.; Hui, C. L.; Hsing, I. M. *J. Phys. Chem. B* **2003**, *107*(40), 11057 – 11064.

[16] Wikander, K.; Ekström, H.; Palmqvist, A. E. C.; Lindbergh, G. *Electrochim. Acta* **2007**, *52*, 6848 – 6855.

[17] Yano, H.; Inukai, J.; Uchida, H.; Watanabe, M.; Babu, P. K.; Kobayashi, T.; Chung, J. H.; Oldfield, E.; Wieckowski, A. *Phys. Chem. Chem. Phys.* **2006**, *8*, 4932 – 4939.

[18] Ng, Y. H.; Ikeda, S.; Harada, T.; Higashida, S.; Sakata, T.; Mori, H.; Matsumura, M. *Adv. Mater.* **2007**, *19*(4), 597 – 601.

[19] Zhang, J.; Lima, H. B.; Shao, M. H.; Sasaki, K.; Wang, J. X.; Hanson, J.; Adzic, R. R. *J. Phys. Chem. B* **2005**, *109*(48), 22701 – 22704.

[20] Service, R. F.; Voss, D. *Science* **1999**, *285*(5428), 682 – 685.

[21] Lim, B.; Jiang, M.; Camargo, P. H. C.; Cho, E. C.; Tao, J.; Lu, X.; Zhu, Y.; Xia, Y. *Science* **2009**, *324*(5932), 1302 – 1305.

[22] Mayrhofer, K. J. J.; Blizanac, B. B.; Arenz, M.; Stamenkovic, V. R.; Ross, P. N.; Markovic, N. M. *J. Phys. Chem. B* **2005**, *109*(30), 14433 – 14440.

[23] Kinoshita, K. *J. Electrochem. Soc.* **1990**, *137*(3), 845 – 848.

[24] Wei, L.; Wang, B.; Wang, Q.; Li, L.; Yang, Y.; Chen, Y. *J. Phys. Chem. C* **2008**, *112*(45), 17567 – 17575.

[25] Warren, S. C.; Messina, L. C.; Slaughter, L. S.; Kamperman, M.; Zhou, Q.; Gruner, S. M.; DiSalvo, F. J.; Wiesner, U. *Science* **2008**, *320*(5884), 1748 – 1752.

[26] Bearden, J. A. *Rev. Mod. Phys.* **1967**, *39(1)*, 78 – 124.

[27] Zschornack, G. *Handbook of X-ray Data, Springer*, Berlin/Heidelberg, 2007.

[28] Izumi, Y.; Obaid, D. M.; Konishi, K.; Masih, D.; Takagaki, M.; Terada, Y.; Tanida, H.; Uruga, T. *Inorg. Chim. Acta* **2008,** *361*, 1149 – 1156.

[29] Izumi, Y.; Nagamori, H.; Kiyotaki, F.; Masih, D.; Minato, T.; Roisin, E.; Candy, J. P.; Tanida, H.; Uruga, T. *Anal. Chem.* **2005**, *77*(21), 6969 – 6975.

[30] Izumi, Y.; Masih, D.; Roisin, E.; Candy, J. P.; Tanida, H.; Uruga, T. *Mater. Lett.* **2007**, *61*, 3833 – 3936.

[31] de Groot, F. M. F.; Krisch, M. H.; Vogel, J. *Phys. Rev. B: Condens. Matter* **2002**, *66*, 195112-1 – 7.

[32] Software package version 2.2.7 based on the works of M. Vaarkamp, H. Linders, and D. Koningsberger.

[33] Siegel, S.; Hoekstra, H. R.; Tani, B. S. *J. Inorg. Nucl. Chem.* **1969**, *31*, 3803 – 3807.

[34] Ankudinov, L.; Ravel, B.; Rehr, J. J.; Condradson, S. D. *Phys. Rev. B* **1998**, *58*, 7565 – 7576.

[35] Ankudinov, A. L.; Rehr, J. J.; Low, J. J.; Bare, S. R. *J. Synchrotr. Radiat.* **2001**, *8*, 578 – 580.

[36] Bazin, D.; Sayers, D.; Rehr, J. J.; Mottet, C. *J. Phys. Chem. B* **1997**, *101*(27), 5332 – 5336.

[37] Safonova, O. V.; Tromp, M.; Bokhoven, J. A. v.; de Groot, F. M. W.; Evans, J.; Glatzel, P. *J. Phys. Chem. B* **2006**, *110*(33), 16162 –16164.

[38] Humbolt, F.; Didillon, D.; Lepeltier, F.; Candy, J. P.; Corker, J. Clause, O.; Bayard, F.; Basset, J. M. *J. Am. Chem. Soc.* **1998**, *120*(1), 137 – 146.

[39] Terheijiden, J.; Van Koten, G.; Van Beek, J. A. M.; Vriesema, B. K.; Kellogg, R. M.; Zoutberg, M. C.; Stam, C. H. *Organometallics* **1987**, *6*, 89 – 93.

[40] Wang, L.; Johnson, D. D. *J. Am. Chem. Soc.* **2007**, *129*(12), 3658 – 3664.

[41] Kruk, M.; Jaroniec, M.; Kim, J. M.; Ryoo, R. *Langmuir* **1999**, *15*(16), 5279 – 5284.

[42] Glatzel, P.; Bergmann, U. *Coord. Chem. Rev.* **2005**, *249*, 65 – 95.

[43] de Groot, F. *Chem. Rev.* **2001**, *101*(6), 1779 – 1808.

[44] Izumi, Y.; Nagamori, H. *Bull. Chem. Soc. Jpn* **2000**, *73*(7), 1581 – 1587.

[45] Izumi, Y.; Kiyotaki, F.; Minato, T.; Seida, Y. *Anal. Chem.* **2002**, *74*(15), 3819 – 3823.

[46] Izumi, Y.; Kiyotaki, F.; Seida, Y. *J. Phys. Chem. B* **2002**, *106*(7), 1518 – 1520.

[47] Izumi, Y.; Masih, D.; Aika, K.; Seida, Y. *J. Phys. Chem. B*, **2005**, *109*(8), 3227 – 3232.

[48] Izumi, Y.; Glaser, T.; Rose, K.; McMaster, J.; Basu, P.; Enemark, J. H.; Hedman, B.; Hodgson, K. O.; Solomon, E. I. *J. Am. Chem. Soc.* **1999**, *121*(43), 10035 – 10046.

[49] Paulus, U. A.; Schmidt, T. J.; Gasteiger, H. A.; Behm, R. J. *J. Electroanal. Chem.* **2001**, *495*, 134 – 145.

[50] Koningsberger, D. C.; de Graaf, J.; Mojet, B. L.; Ramaker, D. E.; Miller, J. T. *Appl. Catal. A* **2000**, *191*, 205 – 220.

[51] Bashyam, R.; Zelenay, P. *Nature* **2006**, *443*(7107), 63 – 66.

[52] Orilall, M. C.; Matsumoto, F.; Zhou, Q.; Sai, H.; Abruña, H. D.; DiSalvo, F. J.; Wiesner, U. *J. Am. Chem. Soc.* **2009**, *131*(26), 9389 – 9395.

Chapter 3

Optimization of Replica Pt–C

3.1 Catalyst designing for high performance PEFC

Dispersed metal nanoparticles play essential roles in petroleum chemistry, electrochemistry, and environmental chemistry and are related to new magnetic materials, fuel cells, and medical applications. Among them, platinum nanoparticles enable various catalytic reactions, e.g. cracking, dehydrogenation, oxidation of hydrogen, reduction of oxygen, and decomposition of nitrogen oxide compounds.

Whereas the chemistry of Pt itself is environment benign, the Pt reserve is limited and the nanoparticles need to be stabilized on/in support, e.g. polymers, carbon, or metal oxides. The catalytic optimization of Pt is not simply to find the best performance per available Pt atoms, but also to reduce the amount of Pt used and/or to maximize the available Pt sites in nanocomposites. In this study, nanocarbon was used as support material for Pt for the decomposition of nitrous oxide.

We previously synthesized Pt particles in narrow particle size distribution centered at 1.2 nm in ordered mesoporous Al–MCM-41[1]. This replica synthesis method has advantages (1) to control the Pt nanoparticle size smaller than the homogeneous pore size of template Al–SiO_2 compounds, (2) catalytically grown support carbon is inherently in close contact with Pt nanoparticles and stabilize them as smaller ones [1], and (3) special morphology can be designed by the choice of template of one- or three-demintinonal ordered meso-pores (Al–MCM-41 versus Al–MCM-48), and (4)

homogeneous Pt particle size and carbon size can be designed due to homogeneous pores. The effects of the Pt content in the Pt–C replica composite and the geometry and size of replica Pt–C on the nitrous oxide decomposition were investigated.

3.2 Synthesis of catalyst

Eeach replica Pt–C composite was synthesize following the scheme shown in Figure 3-1.

3.2.1 Synthesis of replica Pt–C composite-M41

Ten milliliters of 7.7 mM aqueous solution of tetraammineplatinum(II) hydroxide hydrate (Strem Chemicals) and 1.0 g of one-dimensional ordered mesoporous silica Al–MCM-41 (molar ratio Al_2O_3/SiO_2 = 1/79, 1.11 wt% Al; Aldrich) were mixed and stirred at 353 K for 2 days. The suspension was filtered, washed, and heated in vacuum at 573 K for 2 h. 200 mg of obtained powder (Pt–Al–MCM-41, 1.3 wt% Pt) was in 30 mL min^{-1} of H^2 (>99.99%; 101 kPa) flow at 573 K for 2 h and then in 200 mL min^{-1} of C_2H_2 (>98%) + N_2 (>99.999%) flow (molar ratio 1:9, total 101 kPa) at 973 K for 1 h. The obtained black powder (0.72 wt% Pt) was treated with 10 mL of hydrofluoric acid (17 wt%; Special Grade, Wako Pure Chemical) for 24 h and the treatment was repeated by three times to give replica Pt–C composite (0.84 wt% Pt). The replica Pt–C composite obtained using MCM-41 is denoted as “replica Pt–C composite-M41”. Amorphous C dissolves in hydrofluoric acid and composite consisting of Pt–graphitic C was preferably obtained [2,3].

The Pt content was increased from 0.84 wt% to 6.1 wt% for the replica Pt–C composite-M41 by increasing the initial concentration of $Pt(NH_3)_4(OH)_2 \bullet nH_2O$ from

7.7 mM to 26 mM. The Pt content in Pt–Al–MCM-41, Pt–C–Al–MCM-41, and final replica Pt–C composite-M41 powder was 5.3, 2.9, and 6.1 wt%, respectively.

3.2.2 Synthesis of Al–MCM-48

Tetraethyl orthosilicate (TEOS, reagent-grade), aluminium isopropoxide (Aldrich), cetyltrimethylammonium chloride ($[CTMA]^+Cl^-$, Tokyo Kasei Co., Ltd.), and cetyltrimethylammonium hydroxide ($[CTMA]^+(OH^-)$, Aldrich) were mixed in deionized water and the solution was stirred for 4 h at 290 K. The molar ratio of Si : Al : $[CTMA]^+Cl^-$: $[CTMA]^+(OH^-)$: water was 1 : 0.025 : 0.7 : 0.3 : 46.5. The gel was heated in a Teflon bottle at 373 K for 10 days. The precipitates were filtered, washed by ethanol, and dried at 373 K. The powder was calcined at 813 K for 6 h. The temperature increased at 1 K min^{-1} until 813 K.

3.2.3 Synthesis of Al–KIT-6

A Triblock copolymer, poly(ethylene glycol)–block–poly(propylene glycol)–block–poly(ethylene glycol) (equivalent to Pluronic P123, Ardrich) was added to H_2O and 35% HCl. After stirring for 4 h, a clear solution was obtained. *n*-Butanol (*n*-BuOH, Ardrich) was then added and the stirring was continued for 1 h. TEOS and $Al(OiPr)_3$ were added to the solution and stirred for 24 h at 308 K. The gel composition was Si:Al:P123:HCl 35%:*n*-BuOH:H_2O = 1:0.025:0.053:1.84:1.3:194. The synthesis was carried out in a closed Teflon bottle. Subsequently, the mixture was heated at 373 K for 24 h. The precipitated material was filtered without washing and then dried at 373 K for 12 h in air. The powder was finally calcined at 813 K for 24 h.

3.2.4 Synthesis of replica Pt–C composite-M48 and replica Pt–C composite-K6

Synthesis of replica Pt–C composite-M48 and replica Pt–C composite-K6 were similar to replica Pt–C composite-M41 (6.1 wt% Pt). The concentration of $Pt^{II}(NH_3)_4(OH)_2 \bullet nH_2O$ was 26 mM and 10 mL of solution was mixed with 1.0 g of three-demintinonal meso-ordered silica Al–MCM-48 or Al–KIT-6. The Pt content in replica Pt–C composite-M48 powder was 7.4 wt% and that in replica Pt–C composite-K6 powder was 11 wt%.

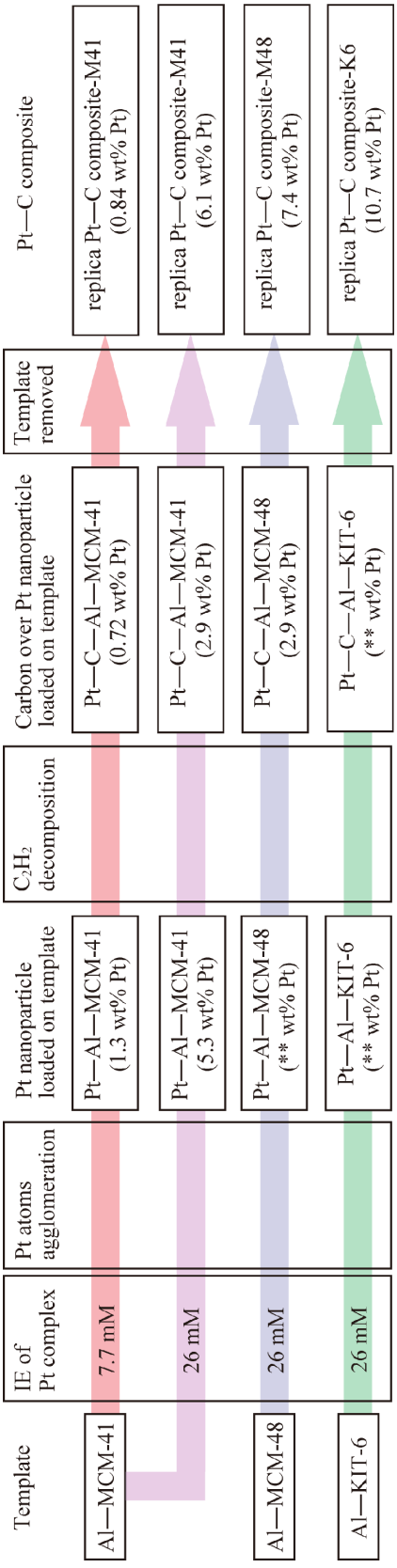

Figure 3-1. Difference of synthesis steps for replica Pt–C composite.

3.3 Characterization for replica Pt–C composites

3.3.1 Phisical property of replica Pt–C composites

Nitrogen adsorption measurements were performed at 77 K with the pressures between 1.0 and 90 kPa in a vacuum system connected to diffusion and rotary pumps (10‑6 Pa) and equipped with a capacitance manometer (Models CCMT-1000A and GM-2001, ULVAC). The samples were evacuated at 393 K for 2 h before measurements. XRD data were obtained using a Rigaku MiniFlex diffractometer at a Bragg angle of 10–75° for crystallines of C and Pt. The conditions involved were 30 kV and 15 mA, Cu K_α emission, and a nickel filter.

High-resolution TEM images were taken using field-emission-type TEM equipment (JEOL, Model JEM-4000FX) with an accelerating voltage of 400 kV for taking the size of Pt particles. Samples were dispersed in ethanol (>99.5%, Wako Pure Chemical) and mounted on amorphous C-coated copper mesh (CU150 Mesh, JEOL).

The Pt content in powder sample was calculated by X-ray absorption of Pt L_3-edge. This measurement was performed at 290 K in the Photon Factory at the High-Energy Accelerator Research Organization (Tsukuba, Japan) on beamlines 7C, 9C and 12C. The X-ray absorption data were analyzed with XDAP (XAFS Services International)[4].

3.3.2 Decomposition reaction tests of N_2O using replica Pt–C composites

Pt–C composite samples were tested for N_2O decomposition. The reaction was performed in a closed circulating system (loop volume 105 mL). 50 mg of Pt–C composites were set into the U-tube connected to the circulation loop. Sample was in vacuum (10^{-6} Pa) at 290 K for 30 min and temperature was raised to 423 K. Then, 30

kPa of N_2O gas was introduced. In every 30 minutes, reactants and products were analyzed using GC-TCD (Shimazu GC-8AT). N_2, O_2, and CO were detected by column of Molecular sieves 13X-S (GL science). Water molecules were detected by column of PEG 6000 (GL science).

3.4 Results

3.4.1 N_2 adsorption results

Nitrogen adsorption isotherms were shown in Figure 3-2. Though there are type IV isotherms and type H3 hysteresis, hysteresis for replica Pt–C composite-K-6 (Figure 3-2c) had two trends divided relative pressure around 0.65. This was indicated difference of pore size of template silica. However, it is nonsense to mention the pore shape of Pt–C composites in detail because it was estimated non-uniform. Replica Pt−C composites were controlled only carbon architecture and uncontrolled pore geometry between the carbon particles. In table 3-1, there were shown BET surface areas and BJH pore volumes calculated by N_2 adsorption. Pore volume of Pt–C composite-M-48 is 0.86 mL g^{-1} which is 1.3 times as large as that of replica Pt–C composite-M-41. Utilizing template silica which has sterically-bulky mesoporous, increasing pore volume of Replica Pt−C composites where reactant gas can be diffused. In contrast, pore volume of Pt–C composite-K-6 is 0. 67 mL g^{-1}. This is suggested too thick pore size of template silica to grow up to 3-dimentional carbon architecture.

3.4.2 XRD results

XRD pattern for replica Pt–C composites were shown in Figure 3-3. The Pt(111)

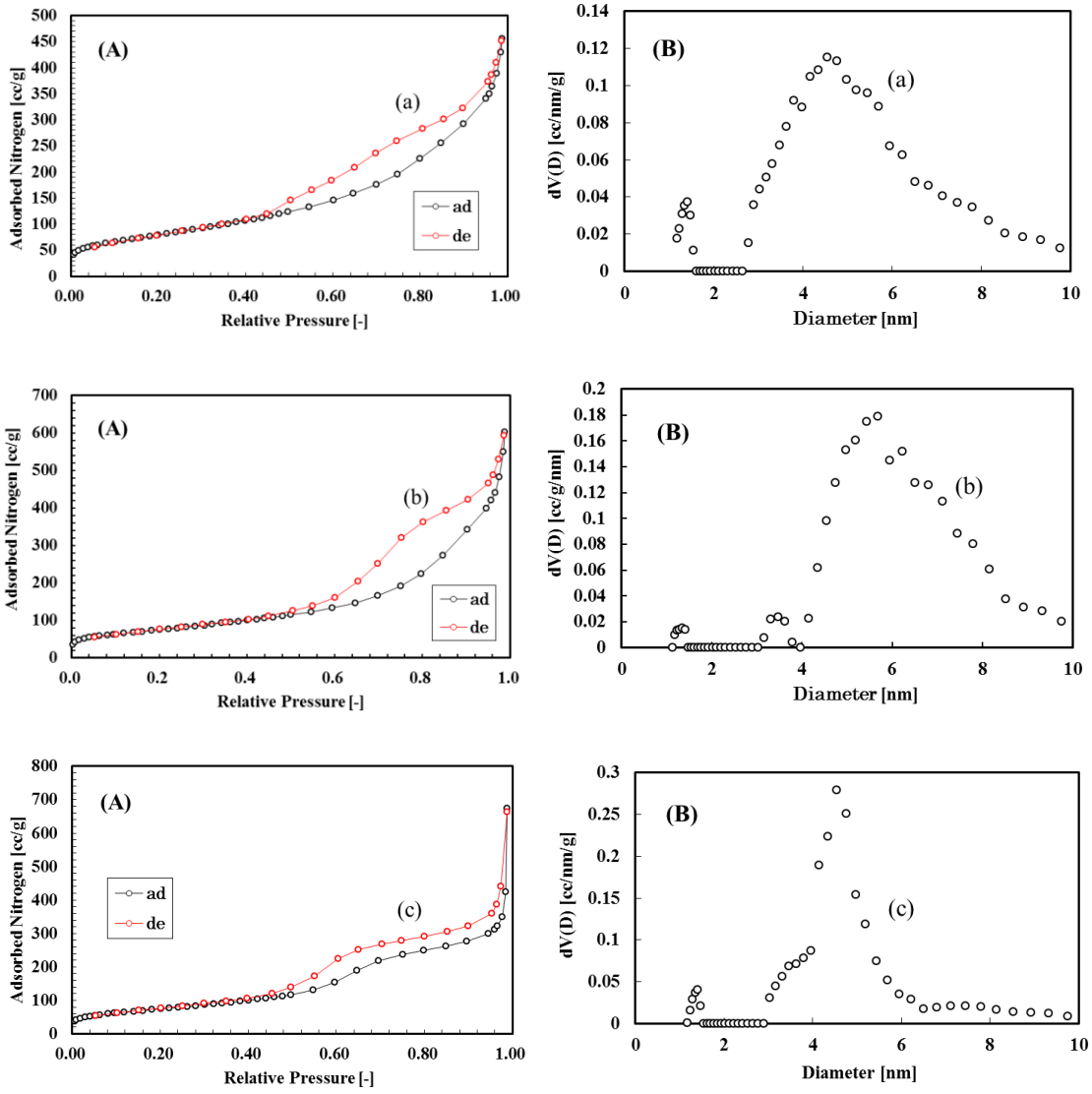

Figure 3-2. Nitrogen adsorption isotherms at 77 K (A) and DFT pore size distributions

diffraction peak was observed commonly at 39.7˚ for spectra a–f. The peak was (B). Replica Pt–C composite-M41 (6.1 wt%) (a), replica Pt–C composite-M48 (b) and replica Pt–C composite-K6 (c). relatively intense for pattern f. C(100) and C(101) diffraction peaks were observed at 42.3˚ and 44.5˚, respectively, for graphitic carbon (reference). The intensity of the two peaks was weak and they merged to one peak at 43˚ between 41–45˚ in Figure 2-3. Broad two peaks of C(100) and C(101) were

Table 3-1: Physicochemical Characterization of Intermediate and Final Materials in the Replica-Pt-C Composite Synthesis

Sample	Pt content (wt%)[a]	d_{Pt} (nm)[b]	Specific S_{BET} ($m^2\ g^{-1}$)	Specific V_{pore}[d] ($mL\ g^{-1}$)	A_C $I_{C(100)/C(101)}$ / $I_{C(002)}$	N_2O decomposition speed ($\mu mol\ h^{-1}\ mg_{Pt}^{-1}$)
Al-MCM-41	—	—	970	1.0	—	—
Pt-Al-MCM-41	1.3	nd.	767	nd.	—	nd.
Pt-C-Al-MCM-41	0.72	nd.	35	nd.	—	nd.
Replica-Pt-C composite-M41	0.84	1.2 (± 0.5)[b]	540	nd.	0.30	nd.
Pt-Al-MCM-41	5.3	nd.	288	nd.	—	nd.
Pt-C-Al-MCM-41	2.9	1.6 (± 0.3)[b]	nd.	nd.	—	nd.
Replica-Pt-C composite-M41	6.1	2.0 (± 0.4)[b]	288	0.68	0.37	3.2
						0.13
Al-MCM-48	—	—	nd.	nd.	—	—
Pt-Al-MCM-48	nd.	nd.	151	nd.	—	nd.
Pt-C-Al-MCM-48	2.9	nd.	nd.	nd.	—	nd.
Replica-Pt-C composite-M48	7.4	1.9 (± 0.4)[b]	268	0.86	0.41	3.1
						0.69
Al-KIT-6	—	—	946	1.2	—	—
Pt- Al-KIT-6	nd.	nd.	nd.	nd.	—	nd.
Pt-C- Al-KIT-6	nd.	nd.	nd.	nd.	—	nd.
Replica-Pt-C composite-K6	11	5.2[c]	270	0.67	0.42	3.5
						0.19
Pt/Ketjen black	39.5	2.7[c]	nd.	nd.	nd.	nd.

[a] Based on Pt L_3-edge jump value. [b,c] Average particle size of Pt based on TEM images[b] or XRD[c]. [d] BJH pore volume.

nd.: not done

merged to one 41–45˚ in Figure 3-3. Broad two peaks of C(100) and C(101) were merged to one peak. This merged peak is indicated planer direction of graphen and C(002) scattering peak ($2\theta_{C(002)}$ = 26.5˚) is indicated layer direction of graphen sheet. The replica Pt–C composites were compared in rate of intensity for C(100)/C(101) merged peak and C(002) peak as indicator of aspect for planer and layer direction of graphen sheet (Table 3-1).

$$A_C = \frac{I_{C(100)/(101)}}{I_{C(002)}}$$

In replica Pt–C composite-M41 (0.84 wt% Pt), A_C was 0.30. The A_C value for replica Pt–C composite-M41 (6.1 wt% Pt) was 0.37. A_C was 0.41 in the replica Pt–C composite-M48 synthesized in three-dimensional ordered mesopore, and slightly greater in direction of graphen planar was obtained in replica Pt–C composite-M48 compered to replica Pt–C composite-M41 (6.1 wt% Pt) which wynthesized from one-dimensional ordered mesopore. In replica Pt–C composite-K6 (Figure 3-3d) which synthesized from thicker three-dimentional mesoporous template, C(100) and C(101) scattering peak was uncertain by high intensity of Pt(111) and Pt(200) scattering peaks. Though, the A_C value for replica Pt–C composite-K6 were almost same to replica Pt–C composite-M48. Thus, three-dimentional template makes graphen planer direction greater carbon. Graphites also deriver the electron to graphen planer direction. However, the A_C values not depended on pore size of template silica.

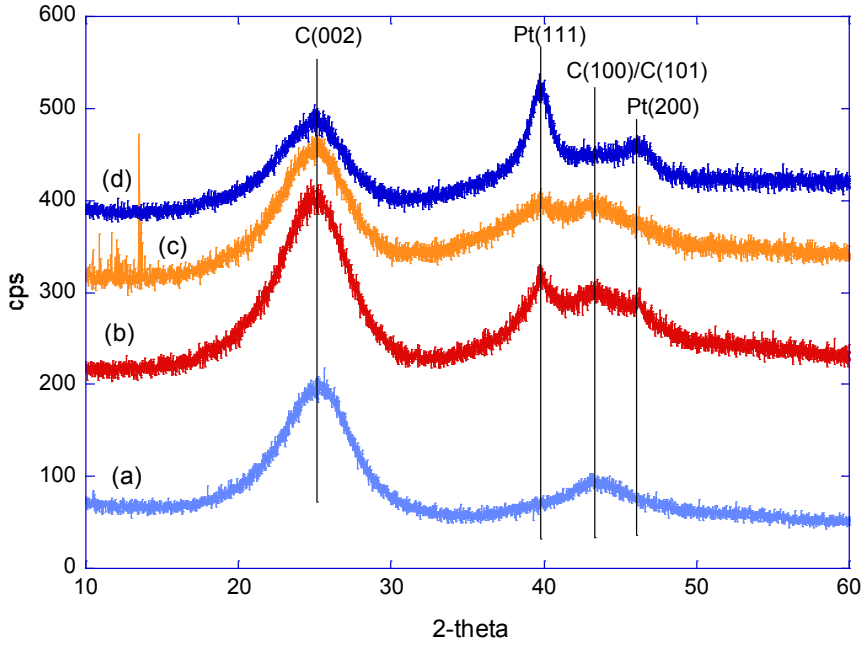

Figure 3-3. XRD patterns for replica Pt–C composite. Replica Pt–C composite-M41 (0.84 wt%, a), replica Pt–C composite-M41 (6.1 wt%, b), replica Pt–C composite-M48 (c) and replica Pt–C composite-K6 (d).

3.4.3 N_2O decomposition results

N_2O decomposition test was performed using each replica Pt–C composites had various carbon architectures. N_2 generation per catalyst platinum weight was shown in Figure 3-4. It was appeared two types of N_2 generation speed per catalyst platinum weight. In the first step, the speed was 2.5–3.2 μmol h^{-1} mg_{Pt}^{-1}. In the second step, the speed decreased to 0.13–0.69 μmol mg_{Pt}^{-1}. According to no generation of O_2, platinum should be oxidized by N_2O. It was estimated surface of platinum particle was oxidized Pt^0 to Pt^{2+} in the first step and internal platinum was oxidized in the second step. N_2 generation using the replica Pt–C composite-K6 (11 wt% Pt) was

shifted to the second step over the 1.3 μmol mg_{Pt}^{-1}. However, N_2 generation using the replica Pt–C composite-M41 (6.1 wt% Pt) or the replica Pt–C composite-M48 (7.4 wt% Pt) was not shifted to the second step until the 3.1–3.2 μmol mg_{Pt}^{-1}. The fact is explainable in terms of platinum particle size. The former has 5 nm platinum particles, the latter has 2 nm platinum particles. The replica Pt–C composite-M41 (6.1 wt% Pt) and the replica Pt–C composite-M48 (7.4 wt% Pt) were higher rate of surface Pt atom than the replica Pt–C composite-K6 (11 wt% Pt). In case of the replica Pt–C composite-M41 (6.1 wt% Pt), N_2 amount was increased and decreased 2.1–4.8 μmol mg_{Pt}^{-1} in the second step. That was indicated gas diffusion was heterogeneously in the space of between the Pt–C composites.

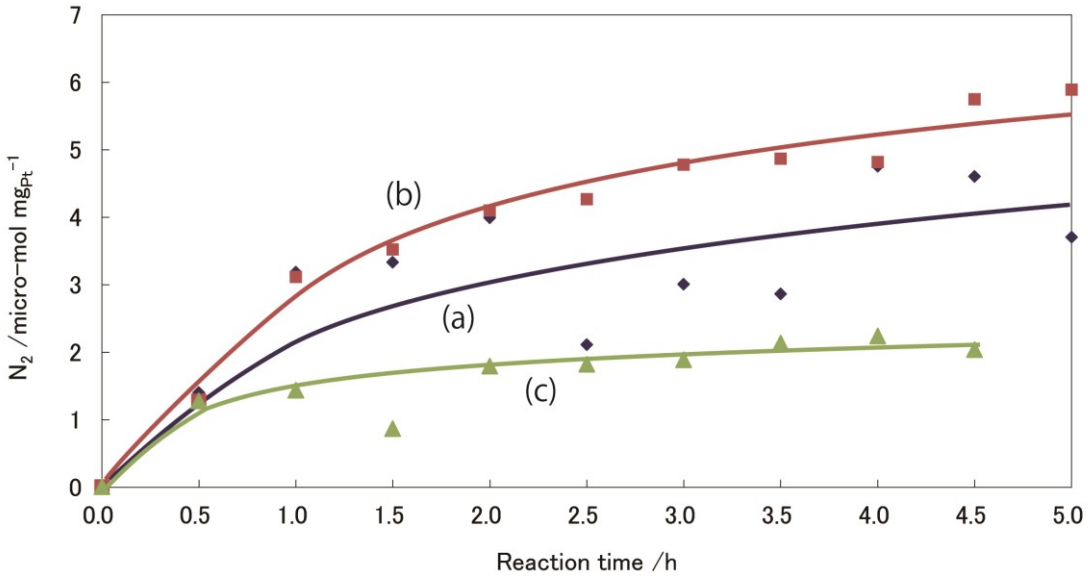

Figure 3-4. N_2 generation amount in N_2O decomposition using replica Pt–C composite-M41 (6.1 wt% Pt, a), Pt–C composite-M48 (7.4 wt% Pt, b), and Pt–C composite-K6 (11 wt% Pt, c) at 423 K.

3.5 Discussions

3.5.1 Increasing the Pt loadings in replica Pt–C composite

Only 2.7% of Pt in Pt–C–Al-MCM-41 (2.9 wt% Pt) was lost during the washing with HF solution, while 47.4% of Pt in Pt–C–Al-MCM-41 (0.72 wt% Pt) was lost. That is because the Pt nanoparticles in Pt–C–Al-MCM-41 (2.9 wt% Pt) were more stable than those in Pt–C–Al-MCM-41 (0.72 wt% Pt) due to greater mean particle size of 1.6 nm compared to 1.2 nm or smaller. After the template silica removed, the ratio of surface Pt atoms which was estimated by the size of Pt particle as the cubo-octahedron was 78 and 57% for replica Pt–C composite-M41 (0.84 wt% Pt) and replica Pt–C composite-M41 (6.1 wt% Pt), respectively. Therefore, replica Pt–C composite-M41 (6.1 wt% Pt) should exhibit by 5.5 times greater catalytic activity than that of replica Pt–C composite-M41 (0.84 wt% Pt).

3.5.2 Difference of pore architectures in template

Template silica was changed from one-dimensional ordered mesoporous silica to three-dimensional that. The surface Pt atom rate in replica Pt–C composite-M48 was 59%. Then, replica Pt–C composite-M48 (7.4 wt% Pt) has 1.3 times as platinum activity area as replica Pt–C composite-M41 (6.1 wt% Pt). Therefore, replica Pt–C composite-M48 has advantage. Figure 3-5 shows carbon architectures models of replica Pt–C composites derived from synthesis method and characterization. Replica Pt–C composite-M41 (6.1 wt% Pt) is estimated one-dimentional carbon architecture transcribed pore architecture of template silica (Figure 3-6A). In contrast, In contrast, replica Pt–C composite-M48 (7.4 wt% Pt) and replica Pt–C composite-K6 (11 wt% Pt) is estimated three-dimentional carbon architecture transcribed pore architecture of

template silica (Figure 3-6-B). The three-dimentional architecture carbon is presumed to difficulty agglutinate because of sterically-bulky. Then, replica Pt–C composite-M48 (7.4 wt% Pt) can ensure N_2O gas diffusion path enough. That is why N_2O decomposition reactivity of replica Pt–C composite-M48 (7.4 wt% Pt) is higher than that of replica Pt–C composite-M41 (6.1 wt% Pt) (Figure 3-5, Table 3-1). Additionally, this information is supported pore volume (Figure 3-2, Table 3-1). It is need to ensure Reactant gas diffusion path in PEFC catalyst. Moreover, energy loss by electrical resistance is estimated to become suppressed for replica Pt–C composite synthesized in three-dimentional pore architecture template (Figure 3-3, Table 3-1). It is necessary to examine replica Pt–C composites utilizing cathode in PEFC, particularly.

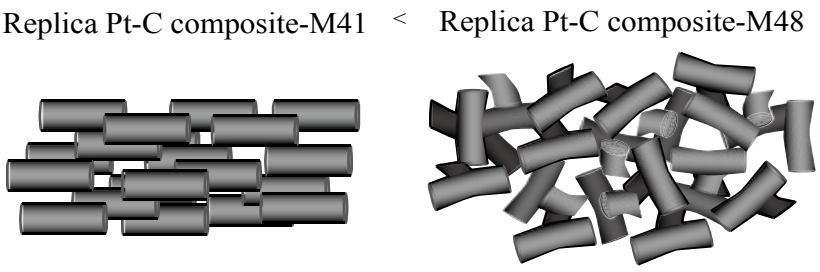

Figure 3-5. Carbon architecture models for replica Pt–C composite

3.6 References

[1] K. Oka, Y. Shibata, T. Itoi, Y. Izumi, *J. Phys. Chem. C* 114 (2010) 1260–1267.

[2] Somanathan, T.; Pandurangan, A. *J. Porous Mater.* **2009**, *16*(4), 459 – 464.

[3] Wei, L.; Wang, B.; Wang, Q.; Li, L.; Yang, Y.; Chen, Y. *J. Phys. Chem. C* **2008**, *112*(45), 17567–17575.

[4] Software package version 2.2.7 based on the works of M. Vaarkamp, H. Linders, and D. Koningsberger.

Chapter 4

Evaluation for triple phase boundary

4.1 Introduction

For polymer electrolyte fuel cells (PEFCs), active site exists at the triple phase boundary in the catalysts.[1] The three phases (solid, liquid, and gas) play the roles of electron conduction, proton diffusion, and reactant gas diffusion, respectively. However, coincidence of the three factors depends on luck during preparation conditions, and triple phase boundary is in general very limited as points. It is important to maximize the boundary between active platinum nanoparticles and proton-conducting polymer. Epting *et al.* observed Pt particle agglomeration and the pore spaces in the Pt/C catalyst layer using 3–dimensional transmission electron microscope (TEM).[2] This is direct evaluation for reactant diffusion path. However, it is still a difficult task to evaluate how much the surface of metal nanoparticle is covered with light and soft constituent, *e.g.* polymer electrolyte. In this work, the boundary formation between Pt nanoparticles and proton conducting polymer was monitored as the electronic state change of Pt by Pt L_3-edge X-ray absorption fine structure (XAFS). The electronic state is sensitive to the surrounding environment, i.e. proton conducting polymer and oxidative/reductive gas. Pt L_3-edge XAFS was recently applied to probe one monolayer of Pt over Rh(111) crystal applied by 0–1.6 V [3].

4.2 Electronic state measurements of Platinum in replica Pt–C catalyst

The replica Pt–C catalyst was prepared following the procedure reported in section 3.2.1. In brief, $Pt(NH_3)_4(OH)_2$ was ion-exchanged with Al–MCM-41 (molar ratio Al_2O_3/SiO_2 = 1/79, 1.11 wt % Al; Aldrich) at 353 K for 48 h. Obtained white powder was heated at 573 K in H_2 and then at 973 K with the flow of acetylene and nitrogen at a rate of 200 mL min^{-1} with the molar ratio of 1:9. Next, Al–MCM-41 template was removed by washing with 15% HF aqueous solution to obtain replica Pt–C powder. Similar synthesis route to this replica Pt–C was also reported using SBA-15 as a template for Pt–C [4] and Pt/Ru–C [5].

50 mg of obtained replica Pt–C-M41 powder (6.1 wt% of Pt) was suspended in 0.2 mL Nafion dispersion solution (diluted to 2.8–1.5% by mixing 5% solution (DE521, Wako Pure Chemical) with ethanol) and dried (replica Pt–C-M41–Nafion). Separately, replica Pt–C-M41 sample was immersed in 0.2 mL of ethanol and dried. Pt supported on Ketjen C black (EC300J) was provided from Ishifuku Metal Ind. (IFPC40-II). Pt L_3-edge XAFS spectra were measured at 290 K in transmission mode in the Photon Factory at the High Energy Accelerator Research Organization (KEK, Tsukuba) on the beamlines of 7C, 9C, and 12C [6,7]. The storage ring was at 2.5 GeV and the current was 180–450 mA. Si(111) double crystal monochromator was used. The data were analyzed using the software package XDAP[8].

4.3 Whiteline peak intensity in the Pt L_3-edge XAFS for Pt samples supported on C

XANES spectra for replica Pt–C with mixing Nafion are shown in Figure 4-1. The intensity of whiteline peaks above the Pt L_3 absorption edge (11562 eV for Pt metal)

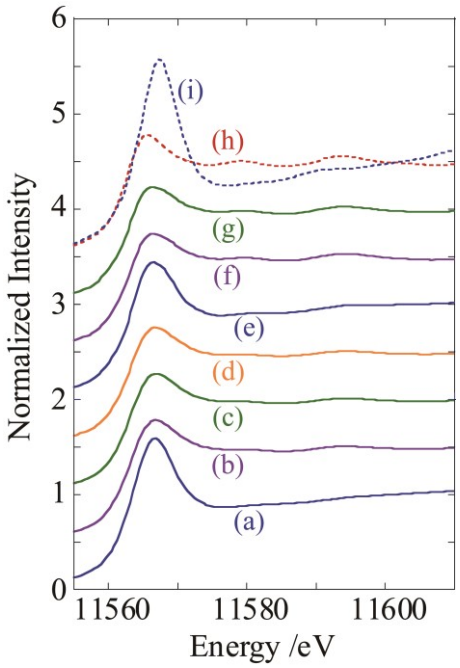

Figure 4-1. Pt L_3 absorption edge XANES spectra for replica Pt–C under air (a), replica Pt–C with 1.5% Nafion and dried (b), replica Pt–C with 2.8% Nafion and dried (c), replica Pt–C in ethanol (d), Pt/C(Ketjen black) under air (e), Pt/C(Ketjen black) with 1.5% Nafion and dried (f), Pt/C(Ketjen black) with 2.8% Nafion and dried (g), 5 mm thick Pt metal foil (h), and PtO_2 (i).

Table 4-1. Energy position (eV) and normalized intensity of whiteline peak at Pt L_3.

	Sample	Energy (eV)	Normalized intensity
(a)	Replica Pt–C-M41 under air	11566.7	1.59
(b)	Replica Pt–C-M41 with 1.5% Nafion after dried	11566.8	1.28
(c)	Replica Pt–C-M41 with 2.8% Nafion after dried	11566.8	1.27
(d)	Replica Pt–C-M41 in ethanol	11566.7	1.26
(e)	Pt/Ketjen black under air	11566.5	1.44
(f)	Pt/Ketjen black with 1.5% Nafion after dried	11566.5	1.24
(g)	Pt/Ketjen black with 2.8% Nafion after dried	11566.4	1.23
(h)	5 μm thick Pt metal foil	11565.6	1.28
(i)	PtO_2	11567.3	2.07

was greater for replica Pt–C-M41 (Table 4-1a) and Pt/C (Ketjen black) (e) under air (1.44–1.59) than 1.28 for Pt metal foil (h). The whiteline peak intensity for replica Pt–C–Nafion (b, c) was 1.28–1.27, lower than 1.44 for replica Pt–C-M41 in air. Immersed in ethanol, the whiteline peak intensity for replica Pt–C (d) decreased to 1.26, that was the smallest intensity among replica Pt–C-M41 samples. The same trend was observed for Pt/C (Ketjen black): 1.44 (under air) > 1.24 (immsersed in 1.5% Nafion and dried) > 1.23 (immersed in 2.8% Nafion and dried) (e–g).

4.4 Correlation between platinum electronic state and Nafion coverage

The changes of whiteline peak intensity above the Pt L_3 absorption edge are explained due to the change of oxidation states of Pt sites by forming the boundary between Pt nanoparticles and Nafion (Figure 4-2). Under air, the valence of surface Pt sites was the mixture of 4+, 2+, and 0 (Figure 4-2A).[9] Similar oxidation/reduction trends of surface sites were monitored based on peaks near the X-ray absorption edges of V, Cu, and Sn K and Au and Pb L_3 [10-17].

Next, the oxidic surface Pt sites were reduced to Pt^0 when the Pt–C catalyst was immersed in Nafion dispersion solution (Figure 4-2B). The reduction was found by the reaction not with Nafion but with alcohols. 26–14% of 1-propanol and 46–72% of ethanol were contained in Nafion dispersion solution used (2.8–1.5%). The Pt sites in replica Pt–C-M41 sample were totally reduced to Pt^0 by just immersed in ethanol based on the whiteline intensity became smaller (1.26) to essentially the same as that for Pt metal (1.28; Table 4-1d, h).

$$m\mathrm{C}_n\mathrm{H}_{2n+1}\text{–OH} + \mathrm{PtO}_m \rightarrow m\mathrm{C}_{n-1}\mathrm{H}_{2n-1}\text{–CHO} + m\mathrm{H}_2\mathrm{O} + \mathrm{Pt}^0 \ (m = 1, 2;\ n = 2, 3, \cdots)$$

Please note that most of Pt sites of replica Pt–C immersed in ethanol were reduced (Table 4-1d) whereas they were re-oxidized to Pt^{2+} and/or Pt^{4+} upon exposed to air based on Pt L_3 XANES. In clear contrast, negligible re-oxidation of Pt^0 was detected when Nafion dispersion solution was used in Pt L_3 XANES (Table 4-1b, c, f, g) probably because Nafion totally covered Pt nanoparticles for the dried replica Pt–C and Pt/C (Ketjen black) samples. Although generally amount of Nafion was used on the cathode in the MEA performance tests to that for X-ray study (Fig. 4-1), but the *in-situ* environment of Pt nanoparticle surface was not exactly identical with the one for dried samples of Table 4-1b, c, f and g because the electrodes during the MEA performance tests were surrounded by pseudo-liquid Nafion aqueous solution.

The reason why the Pt/C(Ketjen black) was more effectively reduced to Pt^0 was considered compared to replica Pt–C once immersed in reductive medium (Table 4-1). The major reason is that the Pt nanoparticles were more surrounded by C atoms synthesized from ethyne gas decomposed over Pt for replica Pt–C and thus the interface Pt sites with C cannot contact with Nafion/alcohol. The interface between Pt and C for replica Pt–C was extensively investigated by state-sensitive Pt L_3-edge XAFS spectroscopy [6].

When samples immersed in 2.8–1.5% Nafion dispersion solution and dried (Table 4-1b, c, f, g), a part of Pt surface covered with Nafion polymer would be remained as Pt^0 and a part of Pt surface exposed air would be reoxidized (Figure 4-2C). Thus, whiteline peak intensity for Pt–C catalyst with Nafion is a nice indicator of the Nafion coverage over the Pt surface and formation of the boundary between Nafion and Pt.

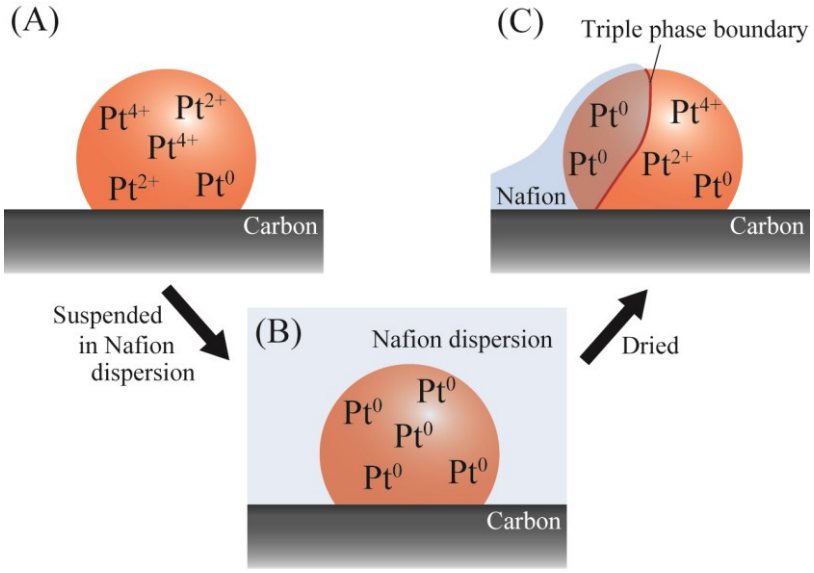

Figure 4-2. Redox of surface Pt in Pt–C catalyst with Nafion. Pt was oxidized under air (A), reduced by alcohol in disperse medium (B), and partially re-oxidized under air (C).

4.5 References

[1] E. Antolini, *J. Appl. Electrochem.*, 34 (2004), 563–576.

[2] W. K. Epting, J. Gelb, S. Litster, *Adv. Funct. Mater.*, 22 (2012), 555–560.

[3] D. Friebel, D.J. Miller, C.P. O'Grady, T. Anniyev, J. Bargar, U. Bergmann, H. Ogasawara, K.T. Wikfeldt, L.G.M. Pettersson, A. Nilsson, Phys. Chem. Chem. Phys. 13 262-266(2011)

[4] J.H. Nam, Y.Y. Jang, Y.U. Kwon, J.D. Nam, Electrochem. Commun. 6, 737-741(2004).

[5] F. Li, K.Y. Chan, H. Yung, C. Yang, S.W. Ting, Phys. Chem. Chem. Phys. 15 (2013), 13570-13577.

[6] K. Oka, Y. Shibata, T. Itoi, Y. Izumi, J. Phys. Chem. C 114 (2010) 1260-1267.

[7] Y. Izumi, T. Itoi, S. Peng, K. Oka, Y. Shibata, J. Phys. Chem. C 113 (2009) 6706-6718.

[8] M. Vaarkamp, H. Linders, D. Koningsberger, XDAP Version 2.2.7, XAFS Services International, Woudenberg, The Netherlands, 2006. http://www.xsi.nl.

[9] Y.-C. Chiang, J.-R. Ciou, *Int. J. Hydrog. Energy*, 36 (2011), 6826–6831.

[10] Y. Izumi, K. Konishi, D. Obaid, T. Miyajima, H. Yoshitake, Anal. Chem. 79 (2007) 6933-6940.

[11] Y. Izumi, H. Nagamori, F. Kiyotaki, D. Masih, T. Minato, E. Roisin, J.P. Candy, H. Tanida, T. Uruga, Anal. Chem. 77 (2005) 6969-6975.

[12] M. Morikawa, N. Ahmed, Y. Yoshida, Y. Izumi, Appl. Catal. B 144 (2014) 561-569.

[13] Y. Yoshida, Y. Mitani, T. Itoi, Y. Izumi, J. Catal. 287 (2012) 190-202.

[14] Y. Izumi, D. Obaid, K. Konishi, D. Masih, M. Takagaki, Y. Terada, H. Tanida, T. Uruga, Inorg. Chim. Acta 361 (2008) 1149-1156.

[15] Y. Izumi, F. Kiyotaki, T. Minato, Y. Seida, Anal. Chem. 74 (2002) 3819-3823.

[16] Y. Izumi, F. Kiyotaki, H. Nagamori, T. Minato, J. Electron Spectrosc. Relat. Phenom. 119 (2001) 193-199.

[17] H. Oyanagi, M. Ishii, C.H. Lee, N.L. Saini, Y. Kuwabara, A. Saito, Y. Izumi, H. Hashimoto, J. Synchrotron Radiat. 6 (1999) 155-157.

Chapter 5

Utilization of proton conductive carbon

5.1 Introduction

Next approach is to maximize the path of electron conducting carbon and proton diffusion. The approach in this work is to functionalize the electron conduction carbon to also conduct protons. Carbon materials functionalized by sulfate group were reported as solid Brønsted acid catalysts.[1-4] The line-like triple phase boundary was expected to extend to face-like by such functionalized carbon material to conduct both electrons and protons was utilized in PEFC.

5.2 Carbon functionalization with sulfate group

5.2.1 Synthesis of HSO_3–C

Five types of carbon powder samples (Ketjen black EC300J, Vulcan XC72R, Darco G-60, Norit SX-Plus, and Norit SX-II) were used as received. 1 gram of carbon powder was doropped into 50 mL of fuming sulfuric acid (15% free SO_3). The suspension in flask was heated at 313–363 K for 10 h with the cooling using reflux condenser. Then, the suspension was filtered by a polytetrafluoroethene-based membrane filter (Omnipore JGWP04700, Millipore) with a pore size of 0.2 μm and washed by hot water (353 K) until the pH of filtrate increased to 6.0. All the procedures were performed under argon atmosphere. Thus-obtained powder is denoted as HSO_3–C (precursor carbon powder name). The proton contents were

determined by titration with sodium hydroxide solution. Namely, slightly excessive sodium hydroxide solution (10 mmol L^{-1}) was added to HSO_3–C powder than to neutralize and well mixed using ultrasonic. The suspension was filtered using a PTFE-based membrane filter (Omnipore JGWP04700). The amount of excessive sodium hydroxide in the filtrate was determined by the titration of oxalic acid solution (10 mmol L^{-1}).

5.2.2 Proton contents in functionalized C with sulfate group

Figure 5-1A illustrates the proton contents in HSO_3–C (Norit SX-II) samples as a function of the heating temperature in fuming sulfuric acid. The proton content in sample was maximized by heating at 353 K (0.49 mmol g^{-1}) and rather decreased to 0.38 mmol g^{-1} when the heating temperature further increased to 363 K. One of the reasons of the decrease was that free SO_3 molecules were liberated to gas phase[5] not to

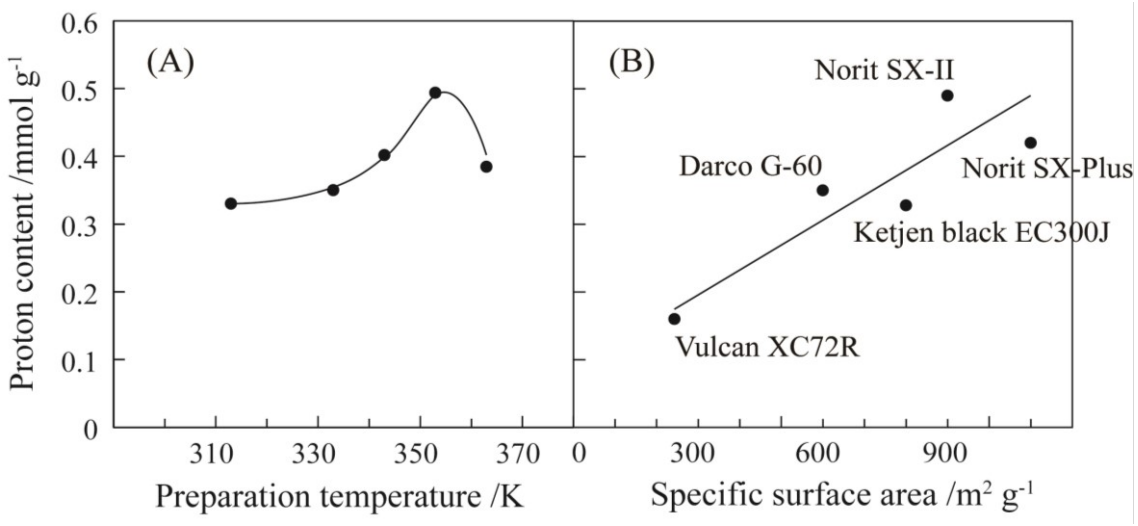

Figure 5-1. Proton contents in HSO_3–carbon as a function of preparation temperature in the range of 313–363 K using Norit SX-II precursor (A) and as a function of specific SA of precursor carbon powder at fixed preparation temperature of 353 K (B).

react with carbon powder anymore. Figure 5-1B depicts proton contents of HSO_3–carbon prepared from several kinds of carbon powders. The proton contents in sample were positively correlated to specific surface area (SA) of precursor carbon powder, indicating that surface sites to react with SO_3 or H_2SO_4 simply increased as the specific SA grew. The edge of graphene sheet is considered as the reacting site with SO_3.[1]

5.3 PEFC performance test

5.3.1 PEFC performance test using cathode catalyst consisting of carbon functionalized with sulfate group

As the cathode of membrane-electrode assembly (MEA), HSO_3–C (Norit SX-II) and/or 0.1 mL of 5% Nafion dispersion (DE521) were mixed with Pt/C (TEC10E50E-HT, Tanaka Precious Metal Ind.; 50.8 wt% of Pt). The polymer amount (4.8 mg) contained in the Nafion dispersion solution was essentially equivalent to the amount (5.2 mg) in 0.2 mL Nafion dispersion solution diluted to 2.8% for replica Pt–C (see section 3.1). The mixing ratios of HSO_3–C, Nafion, and Pt/C were listed in Table 5-1, entries 1–4. The mixture was mounted in the area of 5 cm^2 on water-repellent C paper (TGP-H-060H, Chemix) and dried.

As the anode of MEA, Pt/C (EC-20-20-7, Electrochem) was mixed with 5% Nafion dispersion (DE521) and dried. Thus-obtained cathode and anode were set on the each side of 50 μm thick Nafion film (NR212, Dupont), and pressed at 2 MPa and 393 K for 2 min using a model SA-302 (Tester Sangyo Co.).

PEFC performance tests were performed equipped with the MEA using functionalized C of HSO_3–C (Norit SX-II) prepared at 353 K (0.49 mmol-H^+ g^{-1}). Obtained MEA was set in a PEFC single cell (Model EFC-05-02, Electrochem) and O_2

and H_2 were flowed with a flow rate of 100 mL min^{-1} to the cathode and anode, respectively, both through water bubbler maintained at 353K (partial pressure of moisture: 47 kPa).

Impedance measurements were performed for two MEA models to evaluate the effects of sulfonate/sulfate functionalization. On cathode, 20 mg of HSO_3–C(Norit SX-II) or C powder (Norit SX-II) was mounted in an area of 5 cm^{-2} on TGP-H-060H. On anode, Pt/C powder (EC-20-10-7) was used in similar manner to the MEA above. The cathode, Nafion film (NR212), and anode were pressed at 2 MPa and 393 K for 2 min using a tabletop press (SA-302). Thus prepared MEA models (effective catalyst area 5 cm^{-2}) were sandwiched by two flat copper plates coated with gold with an area of greater than 5 cm^{-2}. An alternating voltage (10 mV) with the frequency of 10^{-2}–10^6 Hz was applied to the MEA model and the impedance and phase angle were monitored using a potentio/galvanostat (Model VersaSTAT3-500 with an option of frequency response analyzer, Princeton Applied Research).

Table 5-1. Contents of cathode layer in MEA.

Entry	Pt/C (mg)	HSO_3–C (Norit SX-II) (mg)	Nafion (mg)	Proton content (μmol)
a	9.8	0	0	0
b	9.9	9.7	0	4.8
c	9.9	0	4.8	4.6
d	9.9	4.8	4.8	7.0

5.3.2 PEFC performance using HSO_3–C (Norit SX-II) and/or Nafion with Pt catalysts

Current–voltage characteristics were tested for PEFC using C(Norit SX-II) functionalized with sulfonate/sulfate and/or Nafion (Figure 5-2). The cell voltage in entry a in which no proton-conducting functional group/polymer was added to Pt/C catalyst (TEC10E50EHT; 50.8 wt% of Pt) in cathode (Table 5-1a) was the lowest and the data values were unstable. This is because the carbon was water-repellent and the protons were conducted to Pt sites only when liquid water was in contact with active Pt nanoparticles.

HSO_3–C (Norit SX-II) was mixed with Pt/C in the cathode for entry b (Table 5-1b). The signal/background ratio in the current–voltage curve was apparently improved compared to data for entry a. It was apparent that HSO_3–C (Norit SX-II) played a role of proton conducting path. However, the cell voltage in entry bwas ~1.6 V lower than that in entry c in which Nafion was used to prepare the cathode Pt/C catalyst instead of mixing HSO_3–C (Norit SX-II) (Table 5-1c, b).

The currentevoltage characteristics were analyzed as a linear fit to the range between 15 and 30 mA cm^{-2} and an extrapolated data of the fit function below the range to current density zero, i.e. voltage axis intercept. The slope evaluated voltage loss dependent on currents and thus should be related to electron and proton conductivity. The voltage axis intercept evaluated overpotential.

The effects of sulfonate/sulfate functionalization were compared to that of Nafion by fixing the proton content (4.6–4.8 mmol) in cathode catalysts (Table 5-1, entry b and c). The slope for entry b (~2.4 V mA^{-1} cm^2) was equivalent or more flat than the one for entry c (~2.7 V mA^{-1} cm^2), but the voltage axis intercept in entry b (0.69 V) was

apparently smaller than the one for entry c (0.85 V). Therefore, HSO_3–C (Norit SX-II) exhibited comparable or slightly better proton conductivity compared to Nafion, but the overpotential was by 0.16 V higher than that using Nafion.

In the entry d, both HSO_3–C (Norit SX-II) and Nafion were mixed to prepare the cathode (Table 5-1d). When 9.7 mg of HSO_3–C was added to 9.9 mg of Pt/C with Nafion, the amount of Nafion suspension solution seemed insufficient to mix well with totally 20mg of powder. Instead, the amount of HSO_3–C for mix was reduced to a half in entry d. The slope was most flat (~2.1 V mA^{-1} cm^2) among all tests in Figure 5-2 and the voltage-axis intercept value was as high as 0.86 V. This was the optimized cathode catalyst in which the boundary between C for the electron conduction and protonconducting polymer was maximized by functionalizing the C surface by

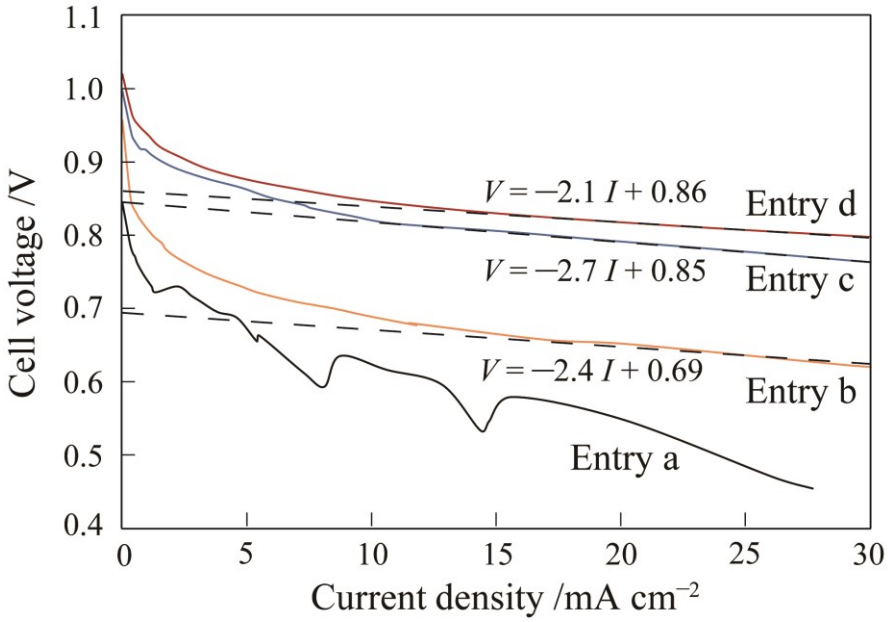

Figure 5-2. Currentevoltage characteristics in MEA performance test. Entry a (black), entry b (orange), entry c (blue), and entry d (red). The dotted lines are the fit in the region between 15 and 30 mA cm^{-2} and the lines were extrapolated to the *V*-axis.

sulfonate/sulfate groups. The currentevoltage characteristics for entries c and d were stable and reproducible in repeated MEA performance tests.

In Bode plot based on the impedance measurements (Figure 5-3A), the impedance for MEA model comprising HSO_3–C (Norit SX-II) was 2.4×10^3 Ω versus 14.2×10^3Ω for MEA model comprising C(Norit SX-II) at 10^{-2} Hz. This impedance difference was a general trend in all the frequency range, suggesting the greater proton conductivity when C surface was functionalized with sulfonate/sulfate. This trend was also supported in Cole–Cole plot (Figure 5-3B). The (part of) impedance circle for MEA model comprising HSO_3–C(Norit SX-II) was apparently smaller than that for MEA model comprising C(Norit SX-II), suggesting smaller impedance (greater proton conductivity) for MEA model comprising HSO_3–C(Norit SX-II).

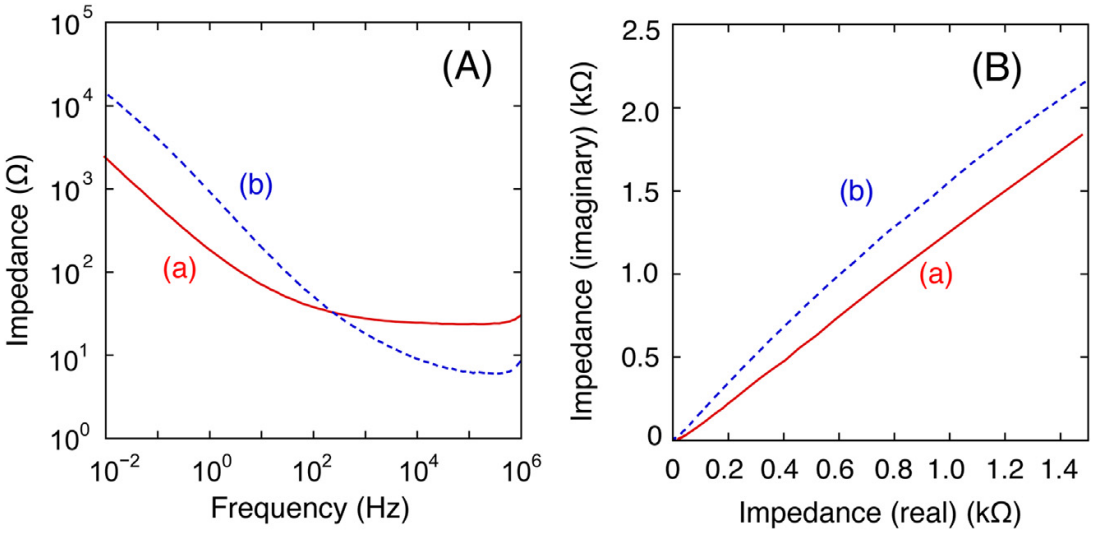

Figure 5-3. Bode plot (A) and ColeeCole plot (B) based on impedance measurements for MEA model using HSO_3–C(Norit SX-II) (a; solid line) and C(Norit SX-II) (b; dotted line) as cathode. Common Pt/C powder (EC-20-10-7) was used as anode.

5.3.3 Efficiency of proton conduction for HSO_3–C and Nafion

Surface-functionalized HSO_3–C (Norit SX-II) was an effective proton conductor to reduce the voltage loss at cathode in the PEFC performance tests (Figure 5-2a, b). Furthermore, impedance measurements for model MEA samples supported improved proton conductance due to the C surface functionalization by sulfonate/sulfate in comparison to bare C black (Figure 5-3a, b).

A proton conduction model in cathode is proposed (Figure 5-4). Using Nafion to prepare the cathode catalyst layer (Figure 5-2c), protons would diffuse by hopping via sulfonate groups of Nafion. Using HSO_3–C (Norit SX-II) in cathode (Figure 5-2b), protons would diffuse also by hopping via sulfonate/sulfate groups of functionalized C. The proton conductivity via HSO_3–C (Norit SX-II) was comparable or slightly superior to via Nafion, but apparently extra energy was required for the proton conduction via HSO_3–C (Norit SX-II) based on the evaluation of overpotential as the voltage-axis intercept values (Figure 5-2b, c). One of the reasons was that the sulfonates of Nafion are neighboring bonded to strong electron withdrawing CF_2 group and would exhibit in strong acid character in contrast that functionalized sulfonate/sulfates bound to C surface should be less acidic for HSO_3–C (Norit SX-II) [6]. Therefore, protons in more acidic medium, i.e. Nafion, were more mobile and leading to smaller overpotential compared to in HSO_3–C.

The major proton conduction path should be via the sulfonates of Nafion in both cases. However, the proton conduction path will be widened by the presence of sulfonate/sulfates of HSO_3–C (Norit SX-II) in addition to Nafion as compared to the interface with Nafion only (Figure 5-4). Further optimization with respect to triple

phase boundary will be expected by functionalizing the C black surface with CF_2-branched sulfonates $(CF_2)_n$ $-SO_3H$ in which equivalent strong acid sites are expected to the side branches of Nafion.

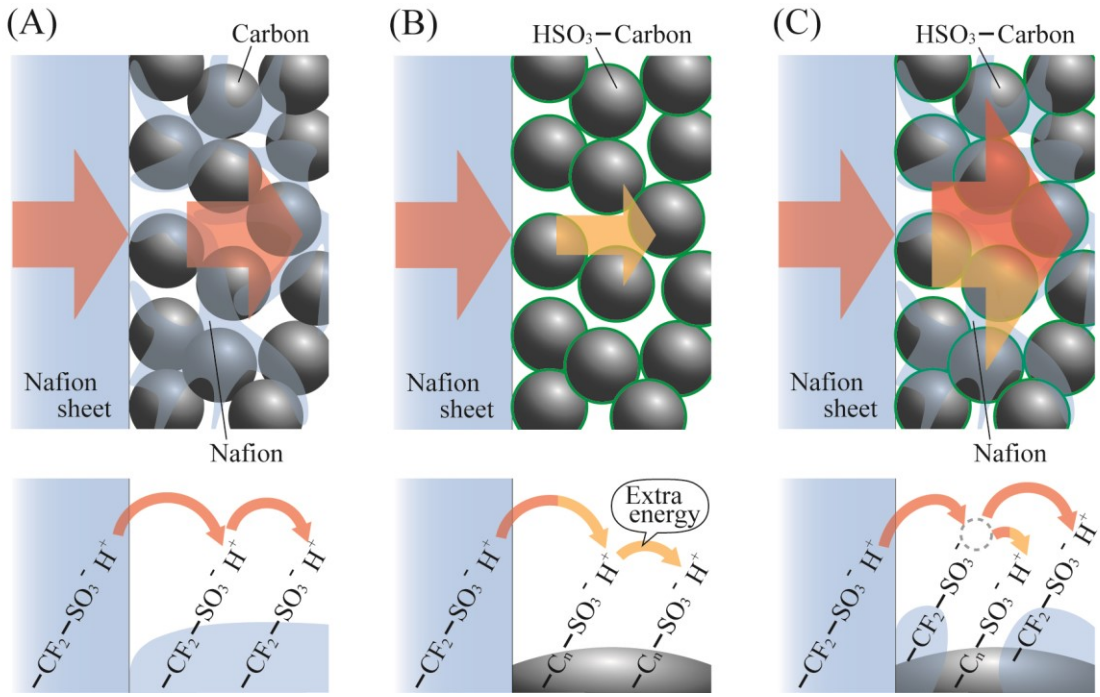

Figure 5-4. Proton delivery in cathode layer including Nafion (A), HSO_3–C (Norit SX-II) (B), Nafion and HSO_3–C (Norit SX-II) (C), respectively.

5.4 References

[1] K. Nakajima, M. Hara, *ACS Catal.*, 2 (2012), 1296–1304.

[2] Q. Shu, J. Gao, Z. Nawaz, Y. Liao, D. Wang, J. Wang, *Appl. Energy*, 87 (2010), 2589–2596.

[3] S. Suganuma, K. Nakajima, M. Kitano, D. Yamaguchi, H. Kato, S. Hayashi, M. Hara, *J. Am. Chem. Soc.*, 130 (2008), 12787–12793.

[4] X. Mo, D. E. López, K. Suwannakarn, Y. Liu, E. Lotero, J. G. Goodwin Jr., C. Lu,

J. Catal., 254 (2008), 332–338.

[5] J. Schrage, *Fluid Phase Equilib.*, 68 (1991), 229–245.

[6] D. A. Evans, The Evans group website, Evans pKa Table, http://evans.harvard.edu/pdf/evans_pKa_table.pdf, 8 Nov. 2013.

Chapter 6

Conclusions

Pt nanoparticles introduced by cation group exchange and formed by heating in vacuum at 573 K inside Al-MCM-41 catalyzed C_2H_2 decomposition to form C rod/tube. The Al-MCM-41 template was removed with 15% of HF solution. Pt nanoparticles with mean size of 1.2 nm were obtained embedded on/in C matrix. The Pt loading was 0.84 wt%. The replica-Pt-C synthetic procedure was supported by the changes of specific S_{BET} value from 767 $m^2\ g^{-1}$ for Pt-Al-MCM-41 to 35 $m^2\ g^{-1}$ for Pt-C-Al-MCM-41 then to 540 $m^2\ g^{-1}$ for replica-Pt-C. The Pt particles could not be monitored by XRD both before and after cathode catalytic tests in PEFC, suggesting the stability of 1.2 nm-Pt particles embedded on/in C matrix. The Pt sites in replica-Pt-C pressed to Nafion were analyzed by Pt $L\beta_1$-selecting high energy-resolution Pt L_2-edge XANES spectra. The first peak above the absorption edge for the spectra tuned to 11065.7 eV was weak, suggesting interface Pt site to receive electron transfer from C in contact. The high energy-resolution XANES spectra both for interfacial Pt with C and metallic Pt sites were nicely reproduced in theoretical spectra generated using FEFF 8.4. The shape resonance peak in H_2 or in air was not certain probably because the anti-bonding levels were below the Fermi level or the shape resonance peaks for H and O_2 adsorbed were similar. Superior turnover numbers were tentatively evaluated for Pt-C-replica in cathode compared to Pt/Valcun XC-72 due to the differences of effective contact of Pt with C *versus* Pt impregnation on C and of diffusion efficiency of fuel O_2 in replica-Pt-C powder.

Optimization of Replica Pt－C composite for PEFC catalyst is done. Replica Pt－C composite-48 is most expected as next generation fuel cell catalyst in the point of high pore volume (0.86 mL g^{-1}), graphitic crystal orientation (A_c = 0.41). N_2 generation in N_2O decomposition reaction (3.1μmol mg_{Pt}^{-1}). However, these are indirection evidence. It is necessary to examine *in-situ* catalyst performance in the early future.

It was possible to maximize the boundary between proton conducting polymer and surface Pt sites based on the synchrotron X-ray monitoring of Pt valence state change dependent on the amounts and concentrations of Nafion dispersion solutions used. Moreover, the support C was functionalized by sulfonate/sulfates to assist the proton conduction via Nafion. Further optimization with respect to triple phase boundary will be expected by functionalizing the C black surface with CF_2-branched sulfonates $(CF_2)_n$–SO_3H in which equivalent strong acid sites are expected to the side branches of Nafion.

Acknowledgements

This work was supported by

Japan Society for the Promotion of Science (JSPS)

KAKENHI Grant Number 24006495 (KO)

Sumitomo Foundation for Basic Scientific Research (No. 070110, YI).

The conventional X-ray absorption experiments were performed under the approval

of the Photon Factory Proposal Review Committee

(No. 2011G523, 2009G531, 2008G167).

The Pt $L\beta_1$ emission and high energy-resolution

Pt L_2-edge X-ray absorption experiments were performed under the approval

of the SPring-8 Program Review Committee (No. 2008B1111).

The author thanks

Dr. Uruga, Dr. Tanida, and Dr. Terada for the adjustment

of beamline optics and technical help at SPring-8.

Prof. Kaneko and Prof. Kanoh for letting us utilize XRD apparatus.

Assoc. prof. Yoshitake for measurement of N_2 sorpotion.

I especially would like to express my deepest appreciation to my supervisor, Assoc. prof. Izumi for providing me this precious study opportunity as a Dr. student in his laboratory.

I am very grateful to labo members for their valuable cooperation in my experiments.

Finally, I express my appreciation to all those who supported me.

Achievements

(1) Paper publication

1. Kazuki Oka[a], Yuta Ogura[b], Yasuo Izumi[d]
   "X-ray evaluation of the boundary between polymer electrolyte and platinum and carbon functionalization to conduct protons in polymer electrolyte fuel cells"
   Journal of Power source, article in press (DOI: 10.1016/j.jpowsour.2014.02.040)

2. Kazuki Oka[a], Yasuo Izumi[d]
   "Preparation and evaluation of boundary between polymer electrolyte and platinum over functionalized proton-conductive carbon"
   IICBEE, 49-51, 2014

3. Seiki Wada[a], Kazuki Oka[a], Kentaro Watanabe[a], Yasuo Izumi[d]
   "Catalytic conversion of carbon dioxide into dimethyl carbonate using reduced copper-cerium oxide catalysts as low as 353 K and 1.3 MPa and the reaction mechanism"
   Frontiers in Chemistry, 1, Article 8 (2013)

4. Kazuki Oka[a], Yoshiyuki Shibata[b], Takaomi Itoi[c], Yasuo Izumi[d]
   "Synthesis and Site Structure of a Replica Platinum—Carbon Composite Formed Utilizing Ordered Mesopores of Aluminum—MCM-41 for Catalysis in Fuel Cells"
   Journal of Physical Chemistry C, **114**, 1260-1267 (2010)

5. Yasuo Izumi[d], Takaomi Itoi[c], Shuge Peng[e], Kazuki Oka[a], Yoshiyuki Shibata[b]
   "Site Structure and Photocatalytic Role of Sulfur or Nitrogen-Doped Titanium Oxide with Uniform Mesopores under Visible Light"
   Journal of Physical Chemistry C, **113**, 6706-6718 (2009)

6. Yasuo Izumi[d], Takaomi Itoi[c], Shuge Peng[e], Kazuki Oka[a], Yoshiyuki Shibata[b]
   "Site Structure and Photocatalytic Role of Sulfur or Nitrogen-Doped Titanium Oxide with Uniform Mesopores under Visible Light"(Erratum)
   Journal of Physical Chemistry C, **113**, 12926 (2009)

7. Yu Mitani[a], Kazuki Oka[a], Yoshiyuki Shibata[b], Kazushi Konishi[a], Diaa Obaid[f], Eri Ishikawa[g], Yasuo Izumi[d], Toshihiro Yamashe[h]
"Monitoring of Photochemical Self-assembly of $[Mo_7O_{24}]^{6-}$ to $\{Mo_{142}\}$-blue Nanoring by Using Mo K-edge XAFS"
Chemistry Letters, **39**, 132-133 (2010)

(2) International conference

Poster presentation

1. ○Kazuki Oka[a], Yasuo Izumi[d]
"Evaluation and optimization of boundary between polymer electrolyte and platinum over functionalized proton-conductive carbon"
International Conference on Biological, Chemical and Environmental Sciences (BCES-2014), Thailand, Jan 2014

2. Yasuo Izumi[d], Kazuki Oka[a], ○Yoshiyuki Shibata[b], Takaomi Itoi[c], Yasuko Terada[i], Hajime Terada[i], Tomoya Uruga[i]
"State-selective monitoring of heterogeneity of gold and platinum nanoparticle catalytic sites related to fuel cells"
14th International Conference on X-ray Absorption Fine Structure, Italy, July 2009